OPTICA
Advancing Optics and Photonics Worldwide

Technical Groups

Subcentimeter Laser Ranging and Its Applications

Featuring John Degnan, Independent Technical Consultant

05 April 2022

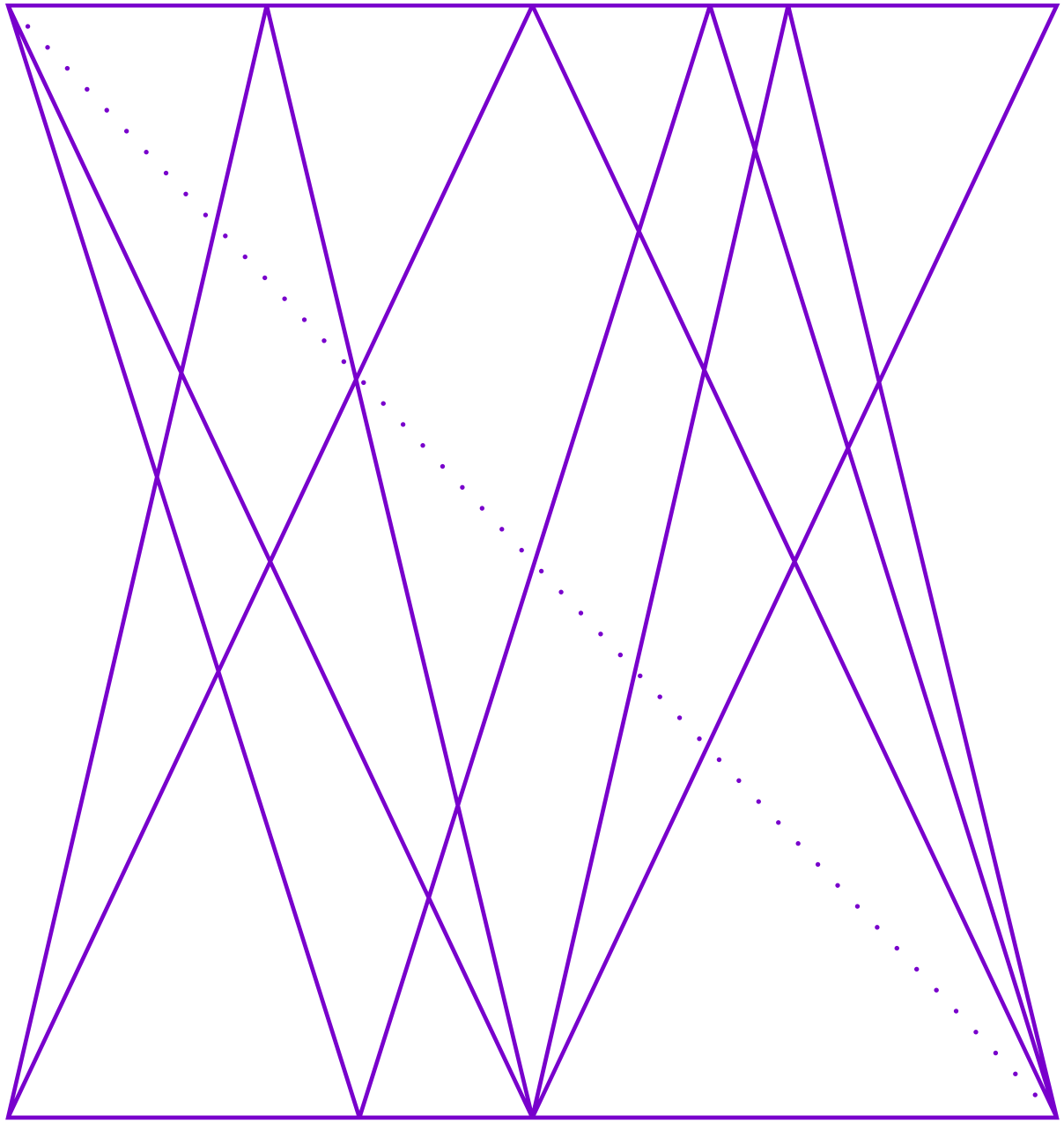

Technical Group Executive Committee

Chair
Dr. Santasri Bose-Pillai
Air Force Institute of Technology

Vice Chair
Dr. Italo Toselli
Fraunhofer IOSB

Webinar & Social Media Officer
Dr. Mark Spencer
Air Force Research Laboratory

Event Officer
Dr. Ferda Canbaz
University of Basel

Event Officer
Dr. Victor Kulikov
University of Dayton

OPTICA
Advancing Optics and Photonics Worldwide
Laser Systems

About Our Technical Group

Our technical group encompasses novel laser system development for a broad range of scientific, industrial, medical, remote sensing and other directed-energy applications.

Our mission is to connect the 4400+ members of our community through technical events, webinars, networking events, and social media.

Our past activities have included:

- Webinar on Turbulence Profile Measurement with a Dynamically Ranged Rayleigh Beacon
- Campfire Session: Breakthrough Starshot Photon Engine
- Webinar on Tailored Gain Materials for Visible and Infrared Lasers

Connect with our Technical Group

Join our online community to stay up to date on our group's activities. You also can share your ideas for technical group events or let us know if you're interested in presenting your research.

Ways to connect with us:

- Our website at www.optica.org/LaserSystemsTG
- On LinkedIn at www.linkedin.com/groups/6993076/
- On Facebook at www.facebook.com/groups/opticalasersystems
- Email us at TGactivities@optica.org

Today’s Speaker

John Degnan

Independent Technical Consultant

Dr. John Degnan is presently a semi-retired Independent Technical Consultant following a 38 year Civil Service career at NASA Goddard Space Flight Center (GSFC) in Greenbelt, MD (1964-2003) and a subsequent 16 year career as Chief Scientist at Sigma Space Corporation in Lanham, MD (2003–2018). Supervisory positions at GSFC included Head, Advanced Electro-Optical Instrument Section; Deputy Manager, NASA’s Crustal Dynamics Project; and Head, Space Geodesy and Altimetry Projects Office. From 1988 to 1992, he also served as a Distinguished Adjunct Professor of Physics at The American University in Washington DC where he taught a two semester graduate course in Quantum Electronics. Dr. Degnan is a Fellow of Optica.

Subcentimeter Satellite Laser Ranging Technology and its Applications

Dr. John J. Degnan

Optica SLR Webinar

April 5, 2022

PART 1:TECHNOLOGY OVERVIEW

- First Successful SLR Experiment at NASA GSFC in 1964
- The SLR Ground Segment
  - Lasers
  - Detectors
  - Time Interval Units and Event Timers
  - Meteorological Subsystems: Surface pressure, temperature, humidity
- Accuracy Improvement: from meters to millimeters over 5 decades
- SLR2000: Single photon ranging at kHz rates
- The Link Equation
- The SLR Space Segment: Retroreflector Array Design
- International Laser Ranging Service (ILRS)
- A Brief Introduction to Lunar Laser Ranging (LLR)
- Interplanetary Laser Ranging, Time Transfer, and Communications via Two-Way Transponders

GSFC records first SLR returns on October 31, 1964

SATELLITE LASER RANGING - 1964

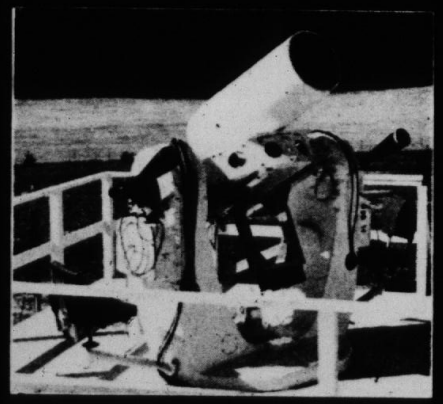

TRANSMITTING LASER AND RECEIVING TELESCOPE, MOUNTED ON A MODIFIED NIKE-AJAX RADAR PEDESTAL.

Code 524 SLR Team

Dr. Henry H. Plotkin
Thomas S. Johnson*
Paul L. Spadin*
John E. Moye*
Walter J. Carrion*
Nelson McAvoy*
Sol Howard Genatt*
Louis O. Caudill
Peter O. Minott
Herbert L. Richards*
Michael W. Fitzmaurice
John J. Degnan
Ed Reid
Charles J. Peruso
Hal Walker*

* Deceased

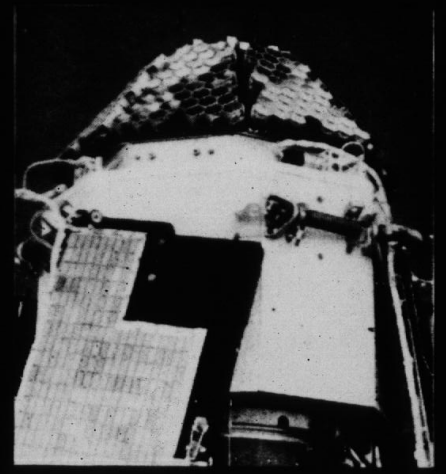

THE BEACON EXPLORER-B SATELLITE WITH ARRAY OF CUBE-CORNER REFLECTORS.

SLR Ground Segment

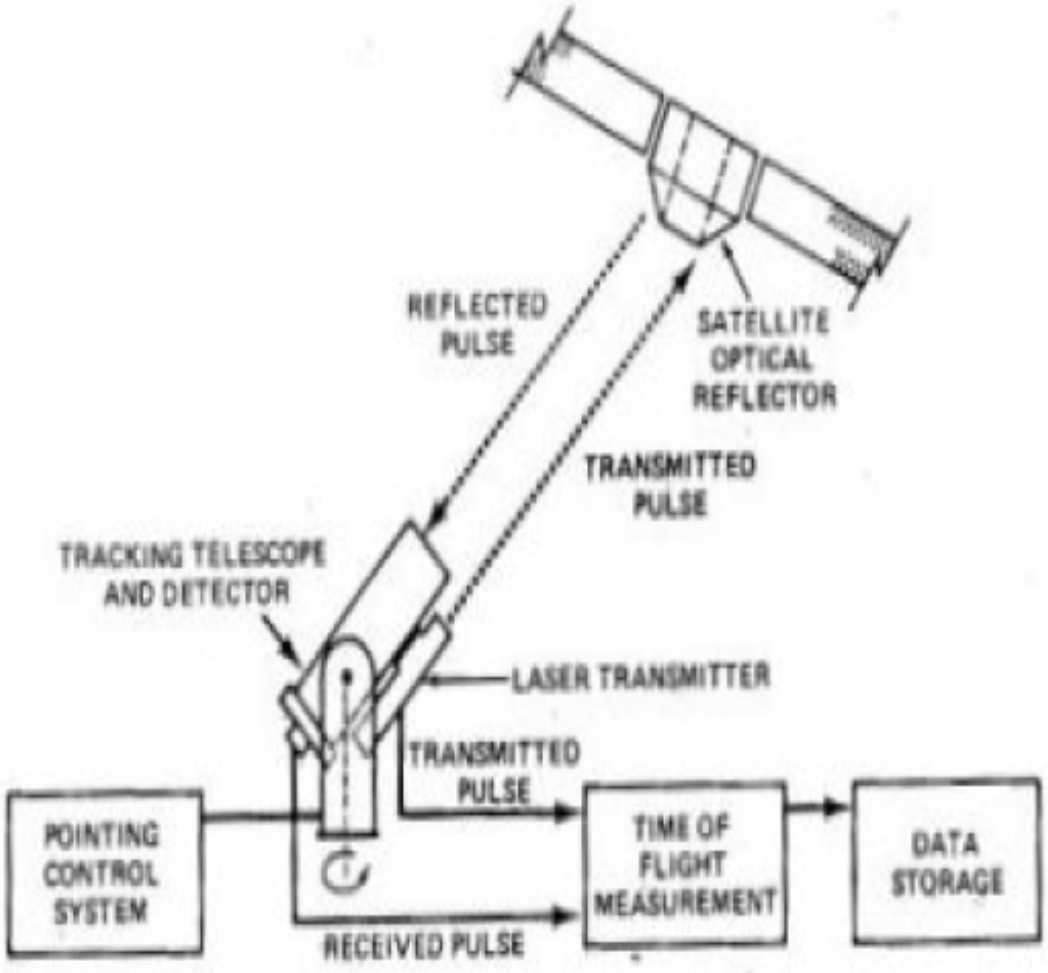

Fig. 1. Satellite laser ranging system concept.

Essential Components

A **laser** which generates a train of short pulses of light

A **telescope, tracking gimbal and control system** to point the laser beam at the satellite and collect the light from the retroreflectors.

A **fast detector** sensitive enough to see the weak signal return from the satellite retroreflector array.

A **Time of Flight (TOF) receiver** which records the times of departure and reception of the laser pulse using an accurate clock.

A **meteorological station** (not shown) to record local surface pressure, temperature, and relative humidity to be input to atmospheric models that provide TOF corrections.

A **data storage unit** to collect and store all of the above data.

Ground Calibration Targets

All SLR stations make use of a calibration scheme to initially determine, and then monitor changes in, optical and/or electronic system delays that might be caused by changes in hardware or environmental conditions (e.g. temperature). The most common approach is to place a single retroreflector at some carefully measured distance from the system "invariant point", defined as the intersection of the elevation and azimuth axes of the telescope assembly. The retro acts as a point source with a delta function response. This distance is usually measured at the 1 or 2 mm level using accurate ground surveying techniques. Subtracting the known target range from the measured range provides a "range correction" which is then applied to all future satellite measurements. For maximum accuracy, ground calibrations are typically performed hourly.

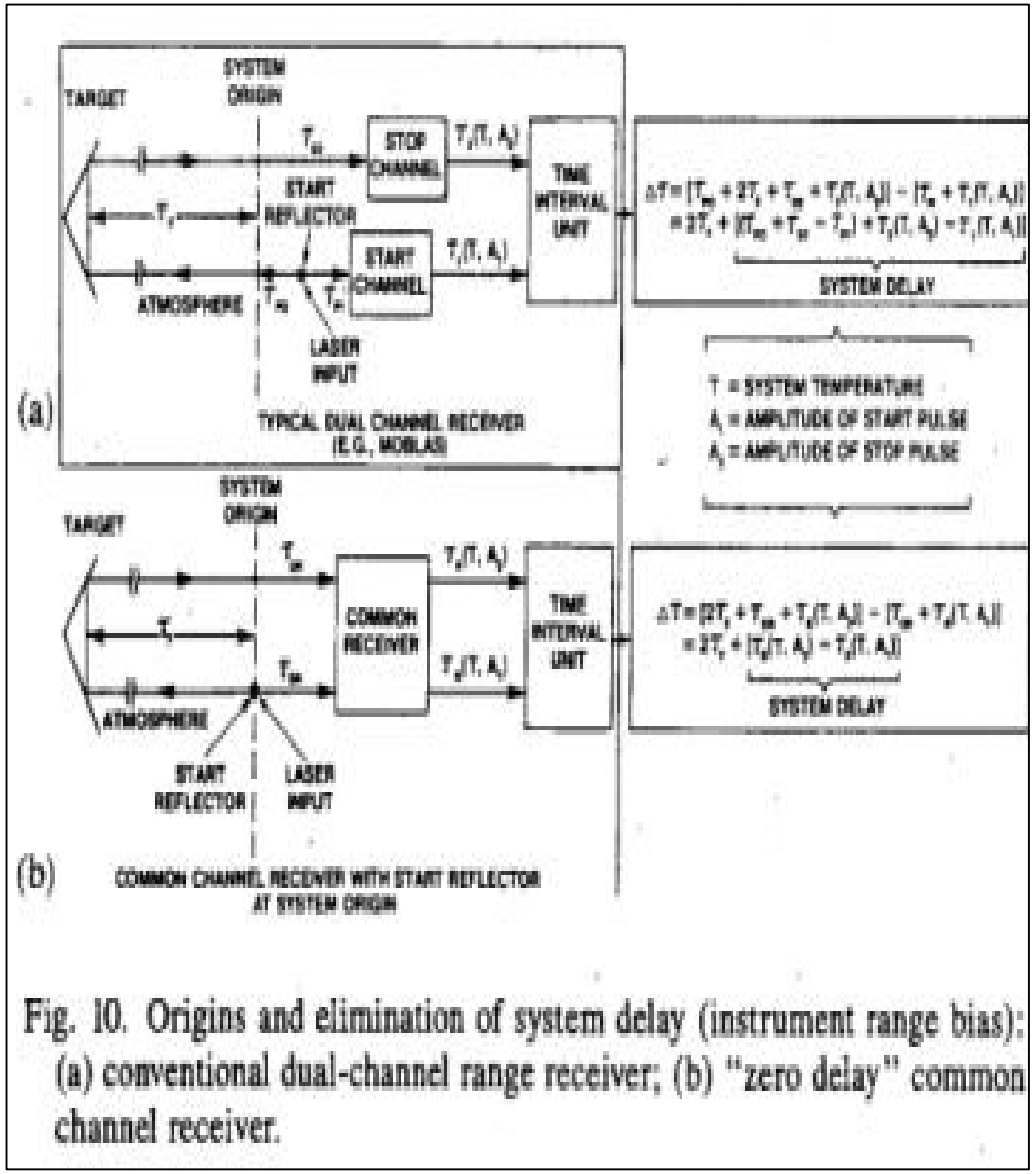

Fig. 10. Origins and elimination of system delay (instrument range bias): (a) conventional dual-channel range receiver; (b) "zero delay" common channel receiver.

SLR Technology in the 1960s

- Laser: Rotating Mirror Q-switched Ruby (694 nm –red beam)
  - Energy: 0.8 J
  - Pulsewidth: 20 nsec
  - Repetition Rate:1 Hz
- Detector: 9558A Photomultiplier – standard dynode chain characterized by large variations in electron propagation paths and large transit time jitter which degraded range precision
- Telescope: 16 inch primary guided by two seated operators on elevation and azimuth joysticks following sunlit satellite image
- No daytime ranging until 1969 when GSFC's Don Premo introduced computer control of the tracking mount.
- Ranging Accuracy improved from 3m to 1m (compared to 50 to 75 m for best microwave radars of the period)
- First generation trailer-based Mobile Laser systems were developed by NASA/GSFC (MOBLAS 1 through 3) and cooperated with two French stations in early science experiments.

Maximizing the Range Precision

We maximize the individual range measurement precision by minimizing the variance in the pulse Time Of Flight (TOF) measurement which is the sum of the variances introduced by the individual subsystems, including the space target, and given by.

$$\sigma_{Total}^2 = \sigma_{Laser}^2 + \sigma_{Detector}^2 + \sigma_{Timer}^2 + \sigma_{T\,\mathrm{arg}\,et}^2$$

Analysts determining the satellite orbits always average over N individual "Full Rate Measurements" to form "Normal Points" for a segment of the orbital arc which have an improved range precision given by

$$\Delta R_{NP} = \frac{\sigma_{Total}}{\sqrt{N}}$$

Thus, as the laser pulse frequency increases, the faster we can achieve the desired normal point range precision. In addition, the resulting normal point can represent a shorter orbital arc length and therefore a higher spatial resolution orbit.

Univ. of Maryland Airborne Atomic Clock Experiment (C. O. Alley et al, 1975)

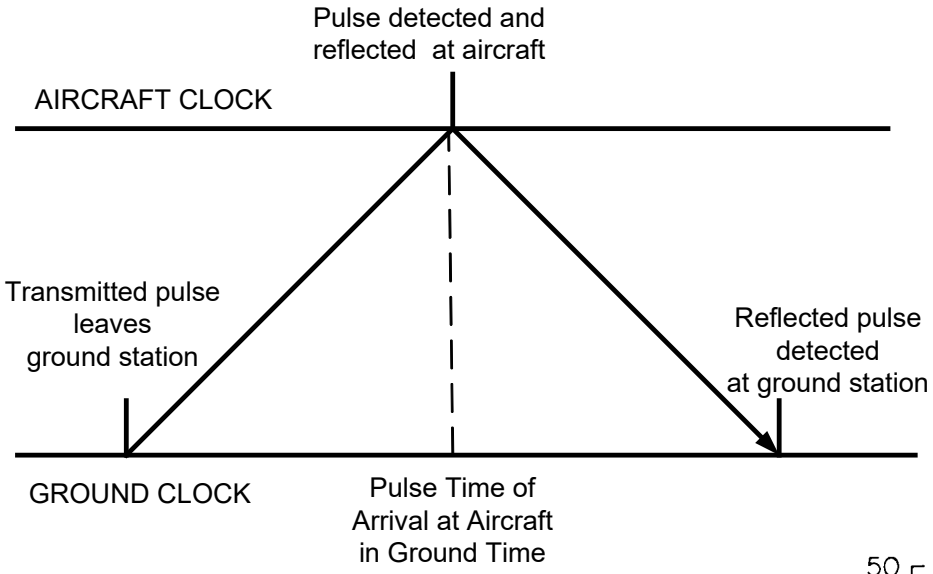

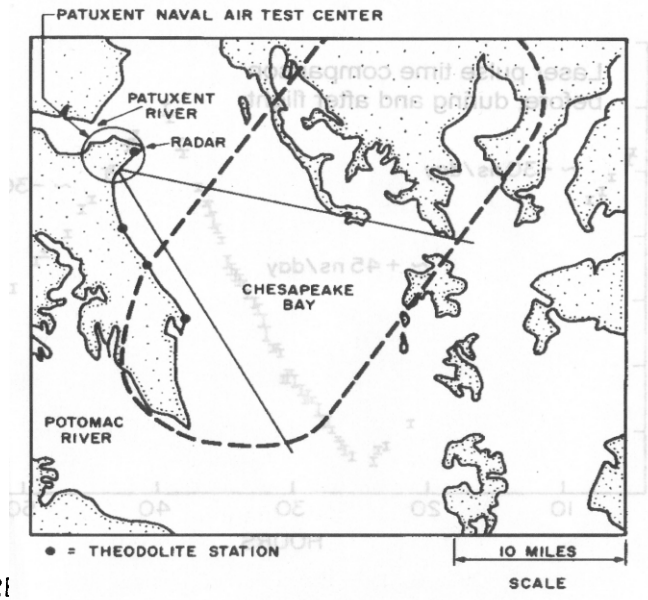

Gravitational redshift	**52.8 ns**
Time dilation	**-5.7 ns**
Net effect	**47.1 ns**

Provided validation of Einstein's theory regarding the relativistic effects of gravity and aircraft velocity on clocks over a 15 hour period!

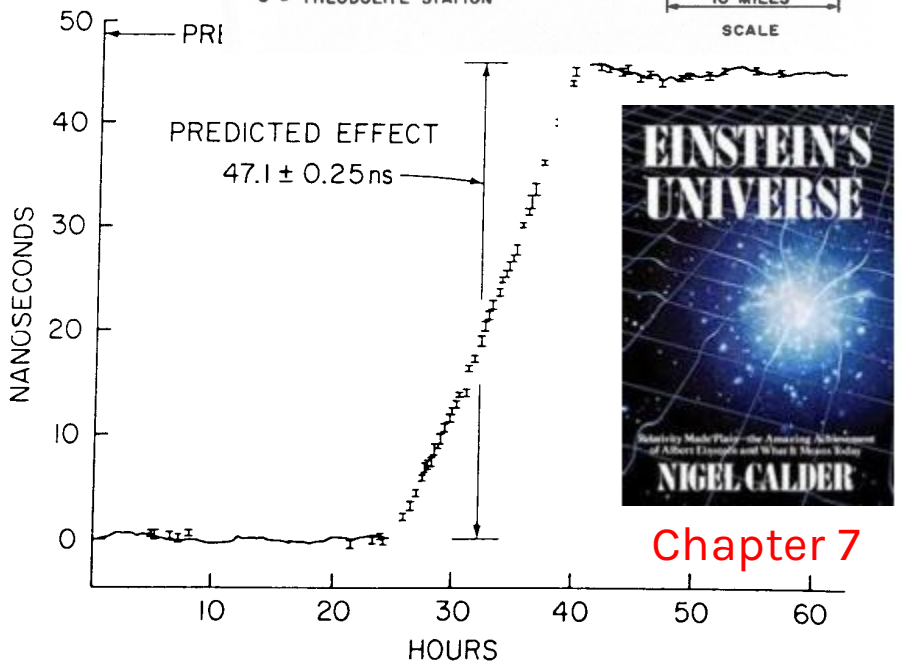

Chapter 7

“World’s Most Expensive Altimeter”

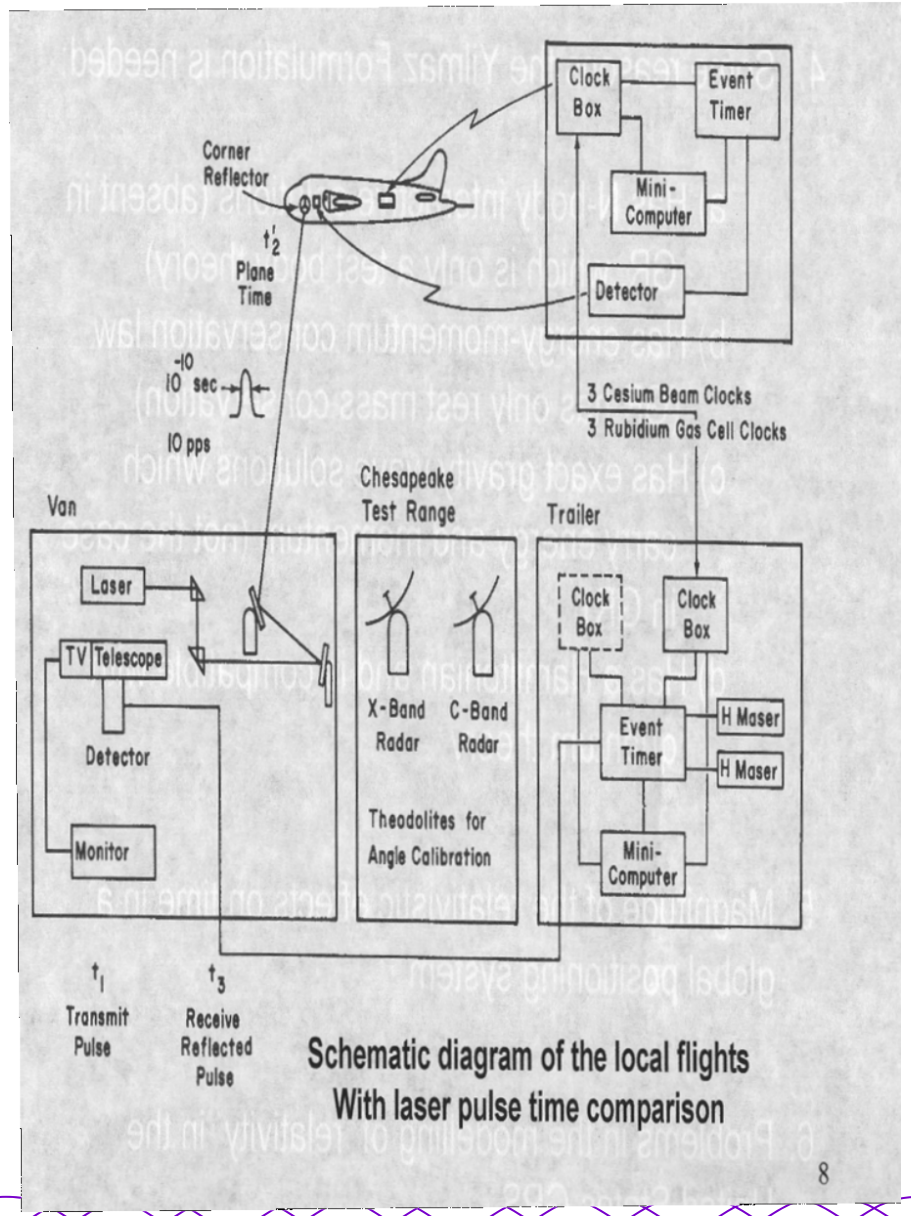

As the aircraft altitude increased, the gravity field weakened and the difference in the ground and airborne clock rates increased as predicted by Einstein.

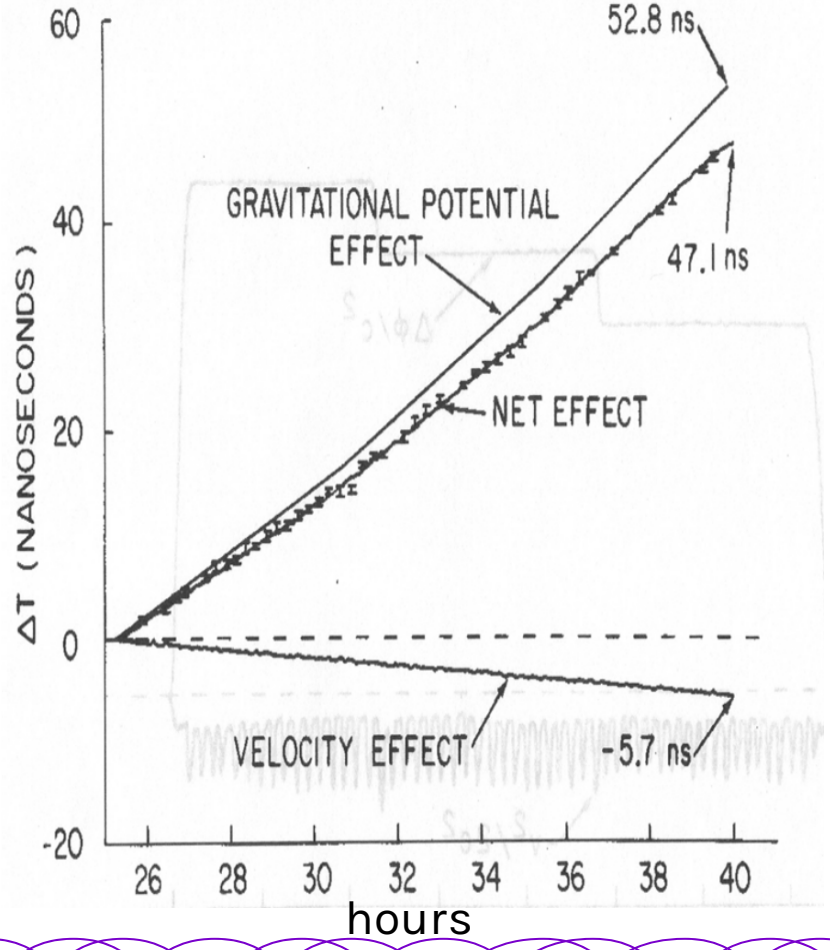

Representative SLR Precision vs Time

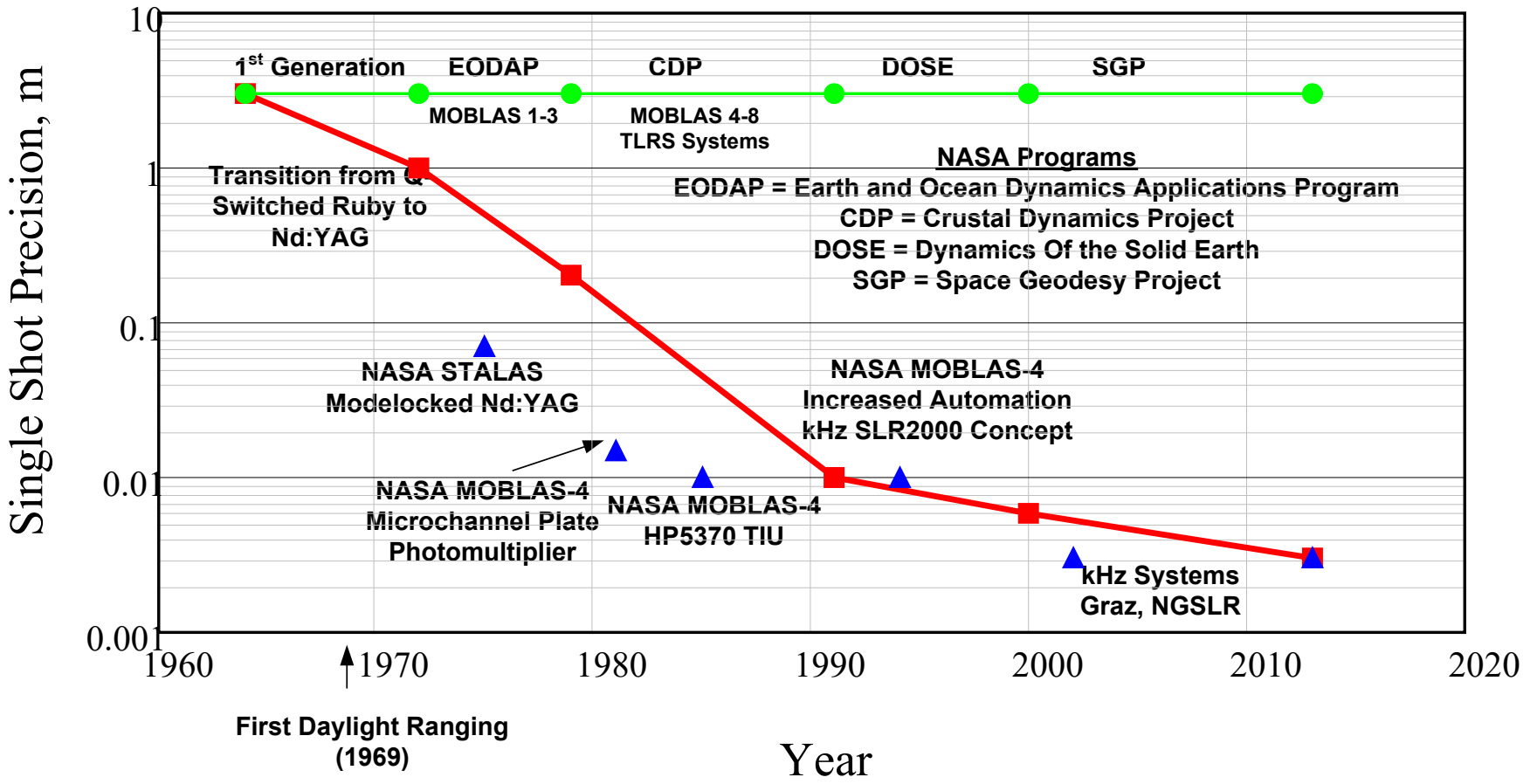

Red Curve = nominal best International SLR Network accuracies vs time

Blue Triangles = key station experiments that eventually led to improved network range performance

SLR2000-NGSLR-SGSLR

McGarry, Hoffman, Degnan ei al,, J. of Geodesy,93(2), Sept.2018

By the 1990s, the growing number of satellites placed a huge financial burden on the international SLR network

SLR2000

- Concept published in 1994 (Degnan), Funding in 1997
- 2 kHz ranging improved normal point resolution by roughly an order of magnitude due to 1/sqrt(N) effect
- Single photon ranging using eyesafe laser beams eliminated need for aircraft safety radars and observers.
- Semi-autonomous operations (1 operator per station per shift vs 3 to 4 for MOBLAS)
- Jan McGarry succeeded Degnan as Project Manager following his retirement from NASA in January 2003

Next Generation Satellite Laser Ranging (NGSLR)

- First satellite tracking at GSFC in March, 2004
- NGSLR was totally destroyed by a lightning strike several years later after successfully tracking all satellites up to GNSS altitudes (23,000 km)

Space Geodesy Satellite Laser Ranging (SGSLR)

- Additional Goals: Fully autonomous operation; 1 mm NP accuracy; lightning protection

SLR2000/NGSLR

SGSLR

Transmit Optical Antenna Gain*

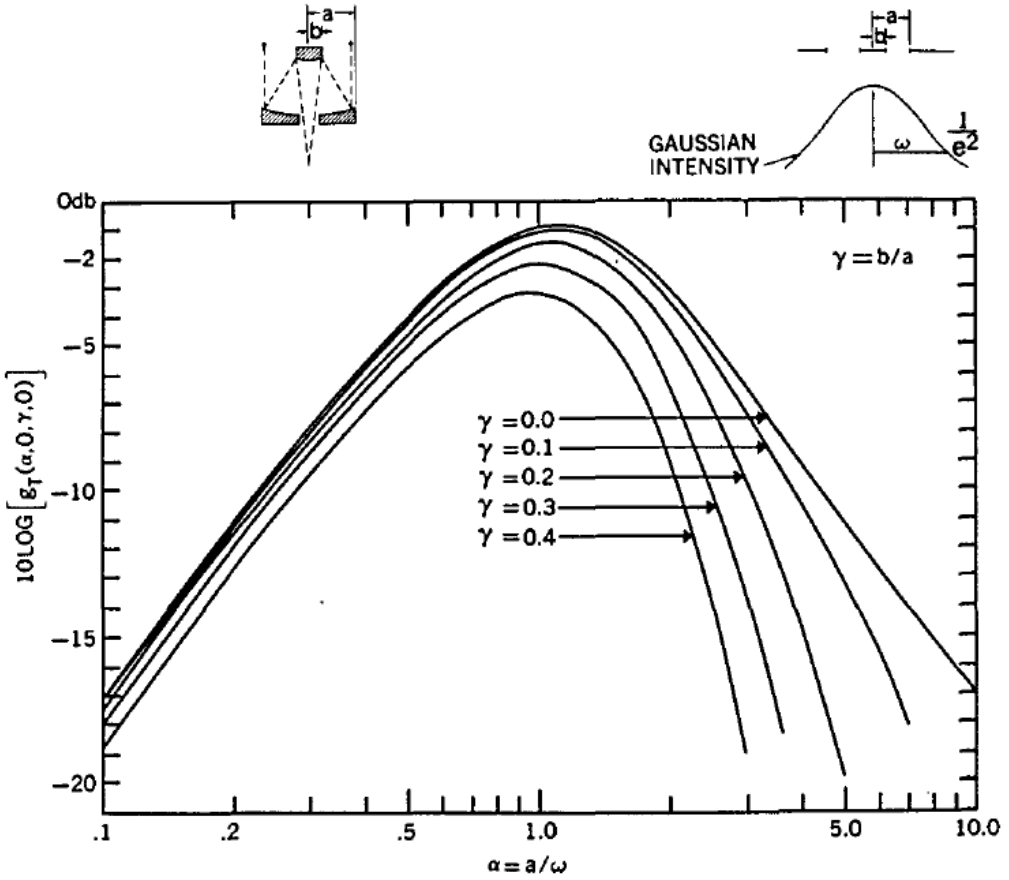

Fig. 3. Far-field axial gain relative to $4\pi A/\lambda^2$ as a function of α for five different obscuration ratios (γ).

One can greatly increase the signal strength at the opposite terminal by optimizing the Gaussian laser beam radius, ω, with respect to the transmit telescope radius, a, and the secondary mirror radius, b (if any). The adjacent plot provides the far-field axial gain as a function of two variables:
α = a/ω and γ= b/a. As the central obscuration becomes larger, the optimum primary to beam diameter ratio (a/ω) becomes smaller but always close to unity.

B. Klein and J. Degnan, Applied Optics, Vol 13, pp. 2134-2141, Sept.1974.

NGSLR Specifications

Variable	Symbol	SGSLR Value
Laser Pulse Energy	E_t	1.5 mJ
Laser Fire Rate	f_L	2 kHz
Transmit Optics Efficiency	η_t	0.77
Receive Optics Efficiency	η_r	0.54
Detector Counting Efficiency	η_c	0.28
Spectral Filter Efficiency	η_f	0.7
Effective Receive Aperture	A_r	0.187 m^2
Tracking Pointing Bias	$\Delta\theta$	2 arcsec (Sigma Receiver)
Telescope RMS Pointing Jitter	$\Delta\theta_j$	2 arcsec
Beam Divergence Half Angle	θ_d	7 arcsec (Starlette, LAGEOS) 3.5 arcsec (GNSS)
Atmosphere and Cirrus Cloud Transmission	Ta and Tc	
Atmosphere Coherence Length (determines Short and Long Term Beam Wander, Scintillation also included in Ta)	ρ_0	2.8 cm (“poor” site) 10 cm (“good” site) 20 cm (“excellent” site)

Range Errors Caused by the Atmosphere

J. Degnan, Millimeter Accuracy Satellite Laser Ranging: A Review, Geodynamic Series Vol. 25, Contributions of Geodesy to Geodynamics, 1993

In addition to instrumental and satellite induced range errors, we have to compensate for few meter level changes in the measured range due to a decreasing atmospheric index of refraction n with altitude which results in changes in the pulse group velocity given by c/n and the deviation of the light path from a straight line The Marini-Murray model assumes the atmosphere consists of thin spherical shells governed by the equations for hydrostatic equilibrium, the law of partial pressures, and the perfect gas law.

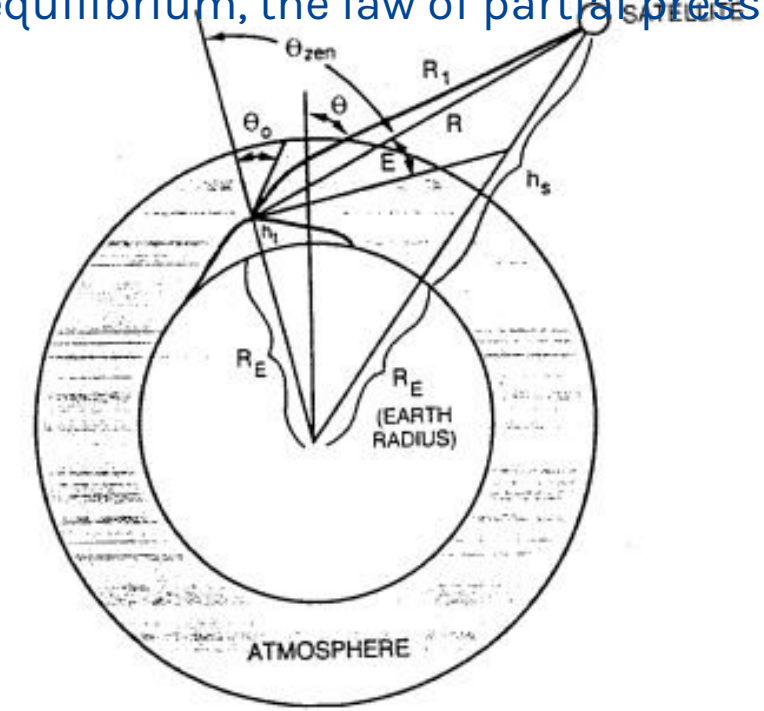

Fig. 15. Coordinate system used in the discussion of atmospheric refraction and the spherical shell model.

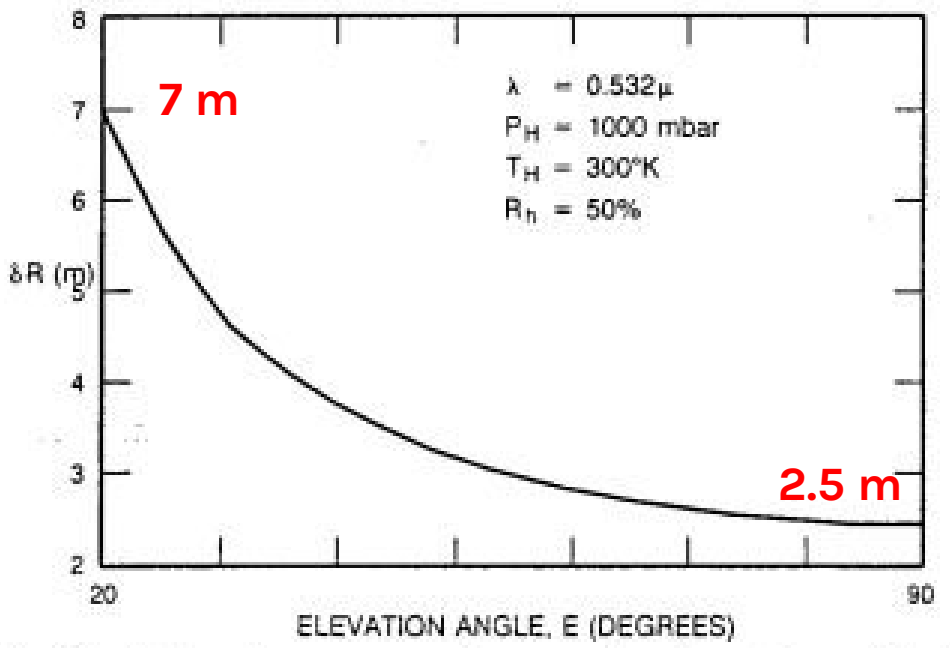

Fig. 16. Single color range correction versus elevation angle as predicted by the Marini-Murray spherical shell model for a wavelength of 532 nm and nominal surface meteorological parameters.

Sensitivity of the Range Error to Meteorological Station Errors

J. Degnan, Millimeter Accuracy Satellite Laser Ranging: A Review, Geodynamic Series Vol. 25, Contributions of Geodesy to Geodynamics, 1993

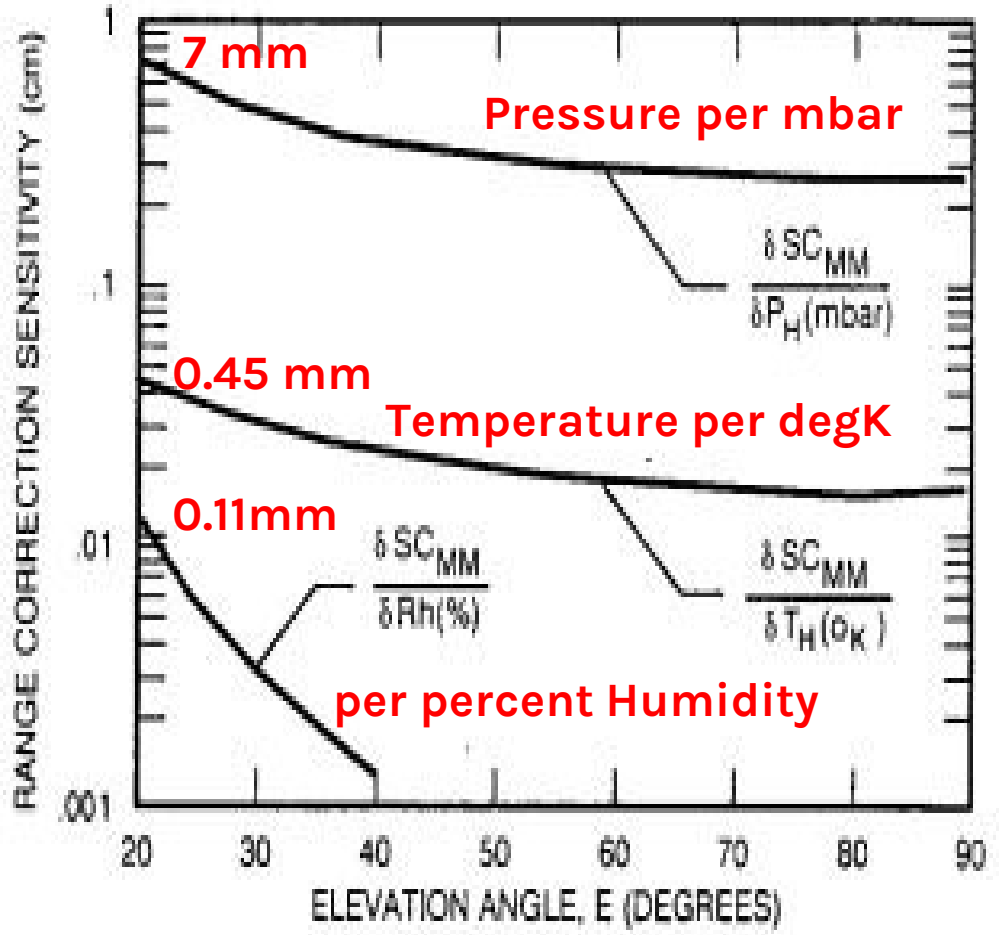

Fig 17. Sensitivity of the Marini-Murray range correction to measurement errors in surface pressure, temperature, and humidity.

NGSLR Meteorological Station

Wind Monitor

- Belfort-Young Model 05103
- Wind speed -Range: 0 to 135 mph; Accuracy: ± 0.6 mph
- Wind Direction: Range: 0 to 360°; Accuracy: +3°

Pressure/Temperature/Humidity Monitor

- Paroscientific MET3-1477-001
- Pressure:Range: 800 to 1100 mbar; Accuracy: ~0.1 mbar; stability<0.1 mbar/yr
- Temperature: Range: -40 to 70 °C; Accuracy<0.5 °C; Stability <0.1 °C/yr;
- Relative Humidity: Range: 0 to 100%; accuracy:±2%; stability: <1%/yr

GPS Antenna

- Receives timing signals from GPS constellation to update Rubidium Frequency Standard and Station Clock

Security Camera

Total Meteorological Range Errors are less than 1 mm!

NGSLR Day/Night All-Sky Cloud Sensor

Uncooled IR Camera

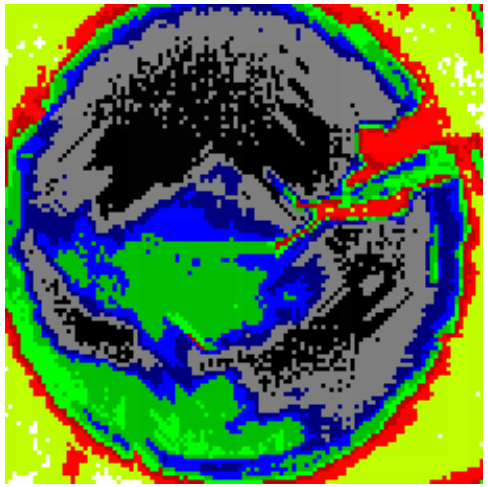

Daytime thermogram shows clear cooler) skies to the north and east. A cloud (warm) covers zenith and extends to the southwest. The red object in the northeast is a support arm. Temperatures are 17 to 33 ^{o}C.

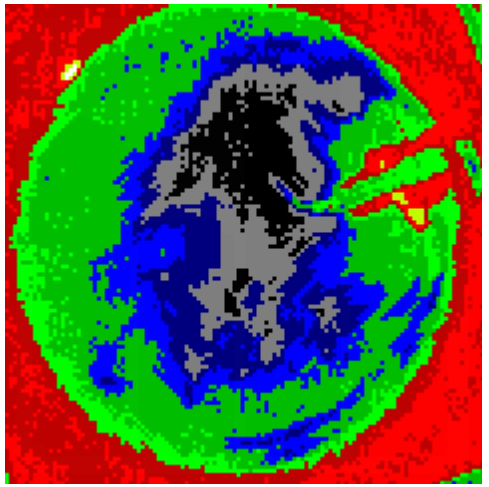

Nighttime thermogram reveals a large patch of clear sky at zenith, extending to the north and south. The east and west are cloudy. Temperature range is 4 to 21 ^{o}C.

Color codes:
warmer = blue, green and red
cooler = gray and black.

NGSLR Precipitation and Visibility Sensing

The Vaisala optics are comprised of an infrared beam and a detector aimed across the beam. Scattering particles in the intersection of the two paths reflect IR light to the detector. These reflections are analyzed and the particles are characterized. The CPU combines this information with temperature data, reports the type and intensity of precipitation, as well as the visibility, and decides whether the dome should be open or closed.

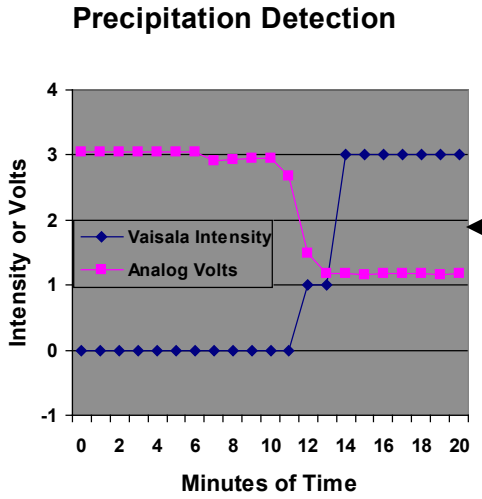

The Vaisala reports precipitation within 2 to 3 minutes of its detection by a sensitive analog device, allowing time to close the dome and protect the equipment.

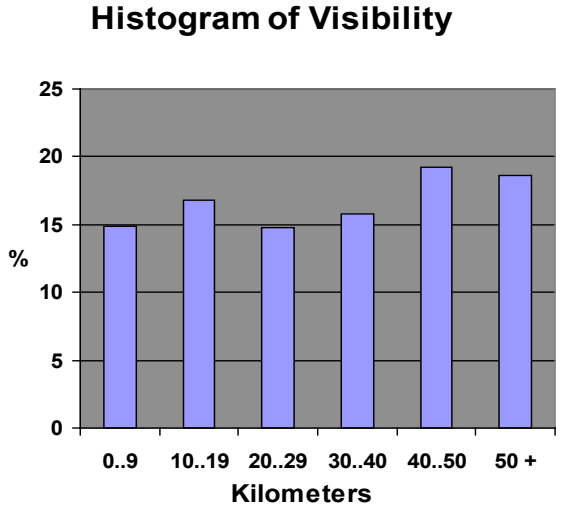

Visibility is defined as the distance that an observer can distinguish a black object against the horizon. At NASA/GSFC, the Vaisala instrument reports a fairly even distribution from 0 to 50 km over a year's time.

Ground Segment Summary

- Minimize laser pulsewidth
  - 1964: Q-switched ruby lasers at 694.3 nm (red) with 20 nsec FWHM pulsewidth
  - Today: Frequency-doubled modelocked Nd:YAG lasers at 532 nm (green) with FWHM pulsewidths <100 psec
- Increase laser pulse rate to accelerate accurate normal point generation and maximize satellite coverage
  - 1964: 1 Hz
  - Today: 2000 Hz (SLR2000, Graz)
- Use fast, low variance (<300 psec) detectors
  - 1964: Dynode Chain PhotoMultiplier Tubes (PMTs) had large electron path variations which degraded accuracy
  - 1981-1985: Replaced by MCP/PMTs (MicroChannel Plate PhotoMultiplier Tubes)
  - Today: Microchannel Plate PhotoMultiplier Tubes (MCP/PMTs), Single Photon Avalanche Photodiodes (SPADs), or Compensated SPADs (C-SPADs) SPAD arrays can also be used to determine satellite position and center the satellite in the telescope FOV for maximum signal
- Use high precision (psec resolution) Event Timers with multistop capability
  - 1964: Single stop Time Interval Units (TIUs) could only make range measurements serially (i.e. single pulse in flight) and therefore limited the rate at which satellite normal point data could be acquired, especially for high altitude satellites
  - Today: Multistop Event Timers (ETs) allow rapid recording of overlapping start and stop events when multiple pulses are simultaneously in flight thereby permitting high altitude satellite tracking at kHz laser pulse rates and reducing the time required for high accuracy Normal Point generation
- Use optimized atmospheric models and high accuracy meteorological measurements (pressure, temperature, and humidity) as inputs for pulse TOF corrections as determined by the Marini-Murray model. More accurate atmospheric models exist for satellite elevation angles below 20 degrees.
  - 1964: Absolute accuracy not particularly relevant due to large instrument errors in the 1 to 3 m range

SLR Link Equation*

$$n_s = \frac{E_t}{h\nu}\eta_t \frac{2}{\pi(\theta_d R)^2}\exp\left[-2\left(\frac{\Delta\theta_p}{\theta_d}\right)^2\right]\left[\frac{1}{1+\left(\frac{\Delta\theta_j}{\theta_d}\right)^2}\right]\left(\frac{\sigma A_r}{4\pi R^2}\right)\eta_r\eta_c T_a^2 T_c^2$$

n_s = detected satellite photoelectrons per pulse
E_t = laser pulse energy
$h\nu$ = laser photon energy = 3.73 x 10^{-19}J @ 532 nm (Doubled Nd:YAG)
η_t = transmitter optical throughput efficiency
θ_d = Gaussian beam divergence half angle
R = slant range between station and satellite (signal decreases as $1/R^4$)
$\Delta\theta_p$ = laser beam pointing error
$\Delta\theta_j$ = RMS tracking mount jitter
σ= satellite optical cross-section = sole link contribution of space segment
A_r = Telescope Receive Area.
η_r= receiver optical throughput efficiency
η_c = detector counting efficiency
T_a = one way atmospheric transmission
T_c = one way cirrus cloud transmission

To maintain the same signal strength, the satellite cross-section must increase as R^4

*Reference: J. Degnan, "Millimeter Accuracy Satellite Laser Ranging: A Review", in Contributions of Space Geodesy to Geodynamics: Technology Geodynamics, 25, pp. 133-162, 1993.

Corner Cube Retroreflectors

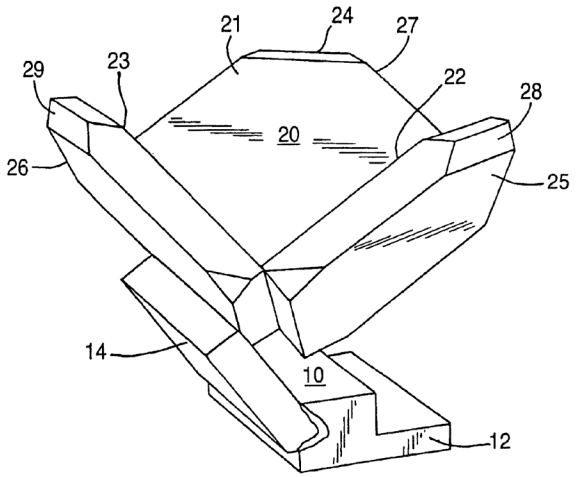

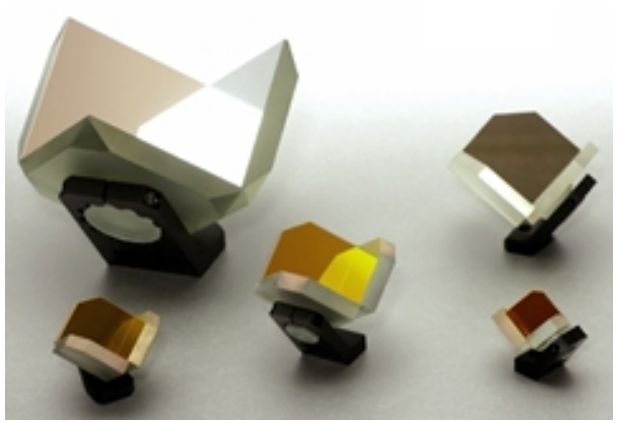

Hollow Cube Corner

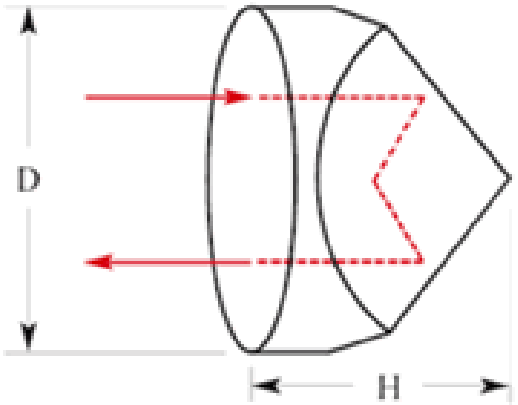

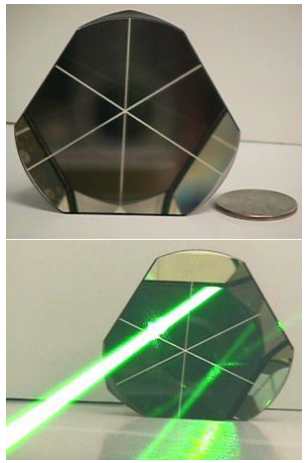

Solid Cube Corner

Cube corner retroreflectors reflect light back to the point of origin in a narrow beam. Increasing the size and/or number of reflectors increases the return signal strength.

Three Types of Cube Corners

Type	Al Back-Coated Solid	Uncoated Solid (TIR)	Hollow
Frequency of Use	Most Common	Occasional Use	Not currently used in the visible
Satellite Examples	Most satellites	Apollo, LAGEOS, AJISAI, ETS-VIII	ADEOS RIS, REM, TES
Reflectivity, ρ	0.78	0.93	Can approach 1.0
Polarization Sensitive	No	Yes	No – metal coating Yes-dielectric coating
Weight	Heavy	Heavy	Light
Far Field Pattern	Wide	Wide	Narrow
Issues	Metal coatings absorb sunlight and create thermal gradients. Not as well shielded at high orbital altitudes.	Fewer thermal problems but TIR "leaks" at incidence angles > 17°. Polarization effects reduce cross-section	Thermal heating and gradient effects on joints

Peak Cross-Section of a Perfect Cube Corner

For normally incident light, a single unspoiled retroreflector (cube corner) has a peak, on-axis, optical cross-section defined by

$$\sigma_{cc} = \rho A_{cc}\left(\frac{4\pi}{\Omega}\right) = \rho\left(\frac{4\pi A_{cc}^2}{\lambda^2}\right) = \frac{\pi^3 \rho D^4}{4\lambda^2}$$

where the reflectivity of the cube corner, ρ, is typically equal to 0.78 or 0.93 for aluminum-coated back faces and uncoated Total Internal Reflection (TIR) surfaces respectively , A_{cc} is the collecting aperture of the corner cube, D is the cube diameter, and $4\pi/\Omega$ is the on-axis reflector gain and Ω is the effective solid angle occupied by the Far Field Diffraction Pattern (FFDP) of the retroreflector.

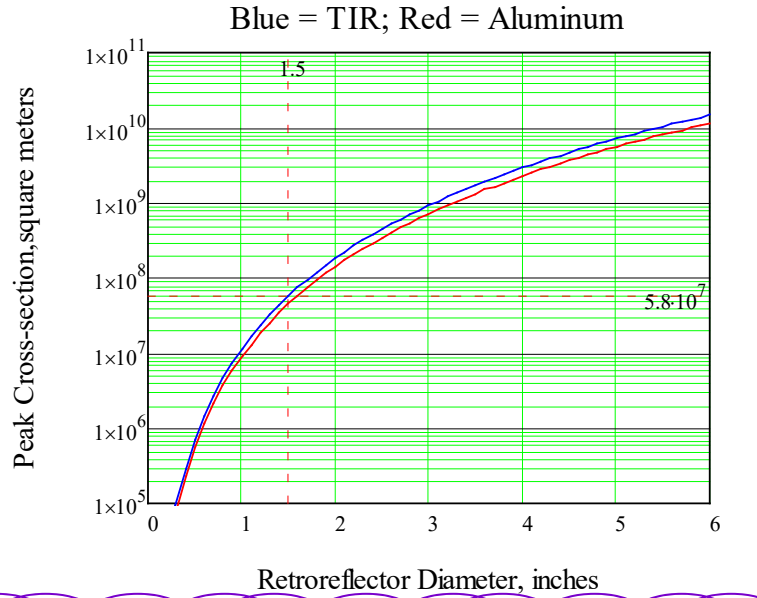

The peak optical cross-section rises rapidly as the retroreflector diameter to the fourth power. For the popular 1.5 in (38 mm) diameter cube with a physical cross-section of 0.001m^2, the peak optical cross-section is about 5.8 x 10^7 m^2, an increase of over ten orders of magnitude.

Retroreflector Far Field Diffraction Pattern(FFDP)

For a uniformly illuminated circular aperture, the FFDP of the reflected wave is the familiar Airy Function given by

$$\sigma(x) = \sigma_{cc}\left[\frac{2J_1(x)}{x}\right]^2$$

where $J_1(x)$ is a Bessel function and the argument x is related to the off-axis angle θ by

$$x = \frac{\pi D}{\lambda}\sin\theta$$

λ = 532 nm is the most widely used SLR laser wavelength, and D is the cube aperture diameter.

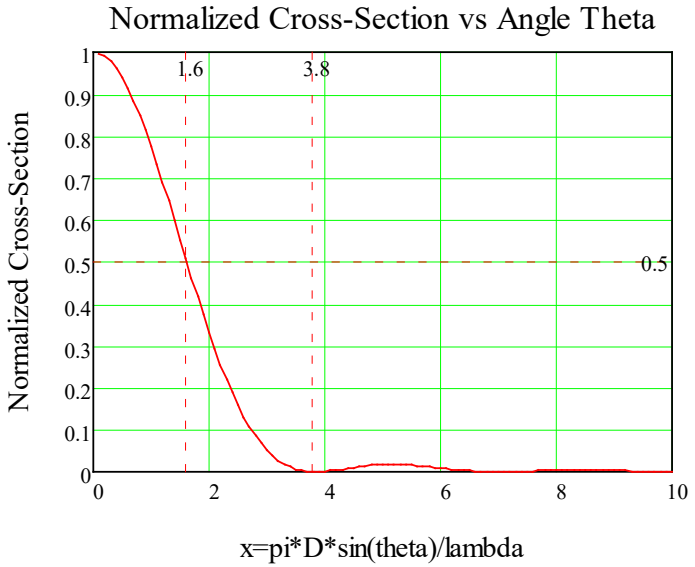

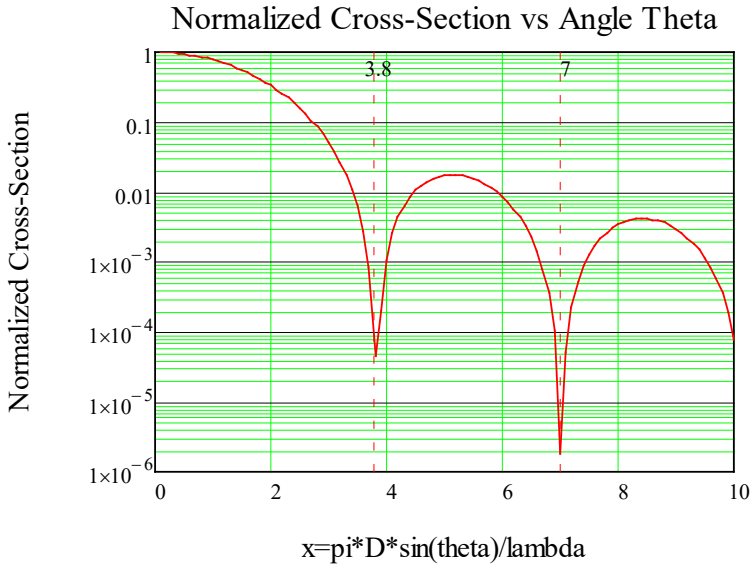

The half-power and first null occur at x = 1.6 and 3.8 respectively. For the popular 1.5 in (38 mm) diameter cube at 532 nm, this corresponds to θ = 7.1 and 16.9 microradians (1.5 and 3.5 arcsec) respectively.

Peak Cross-Section vs Incidence Angle (Hollow Cube vs Coated Fused Silica)

At arbitrary incidence angle, θ_{inc}, the effective area of the cube is reduced by the factor

$$\eta(\theta_{inc}) = \frac{2}{\pi}\left(\sin^{-1}\mu - \sqrt{2}\tan\theta_{ref}\right)\cos\theta_{inc}$$

where θ_{inc} is the incidence angle and θ_{ref} is the internal refracted angle as determined by Snell's Law, i .e.

$$\theta_{ref} = \sin^{-1}\left(\frac{\sin\theta_{inc}}{n}\right)$$

where n is the cube index of refraction. The quantity μ is given by the formula

$$\mu = \sqrt{1 - \tan^2\theta_{ref}}$$

Thus, the peak optical cross-section in the center of the reflected lobe falls off as

$$\sigma_{eff}(\theta_{inc}) = \eta^2(\theta_{inc})\sigma_{cc}$$

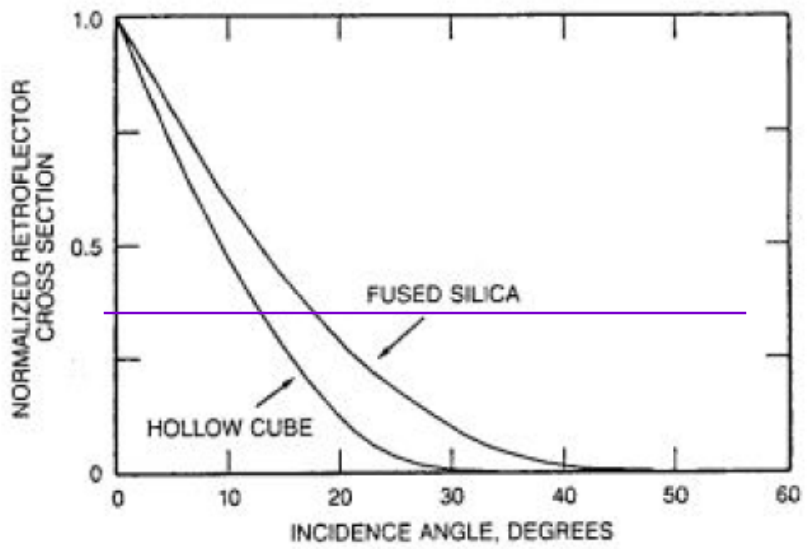

Fig. 23. Normalized cross-section as a function of incidence angle for hollow and fused silica retroreflectors.

- **The 50% and 0% efficiency points for fused silica (n=1.455) are 13° and 45° respectively.**
- **The 50% and 0% efficiency points for a hollow cube (n=1) are 9° and 31° respectively.**
- **In short, hollow cubes have a narrower angular response range than solid cubes.**

Effect of Incidence Angle on the FFDP

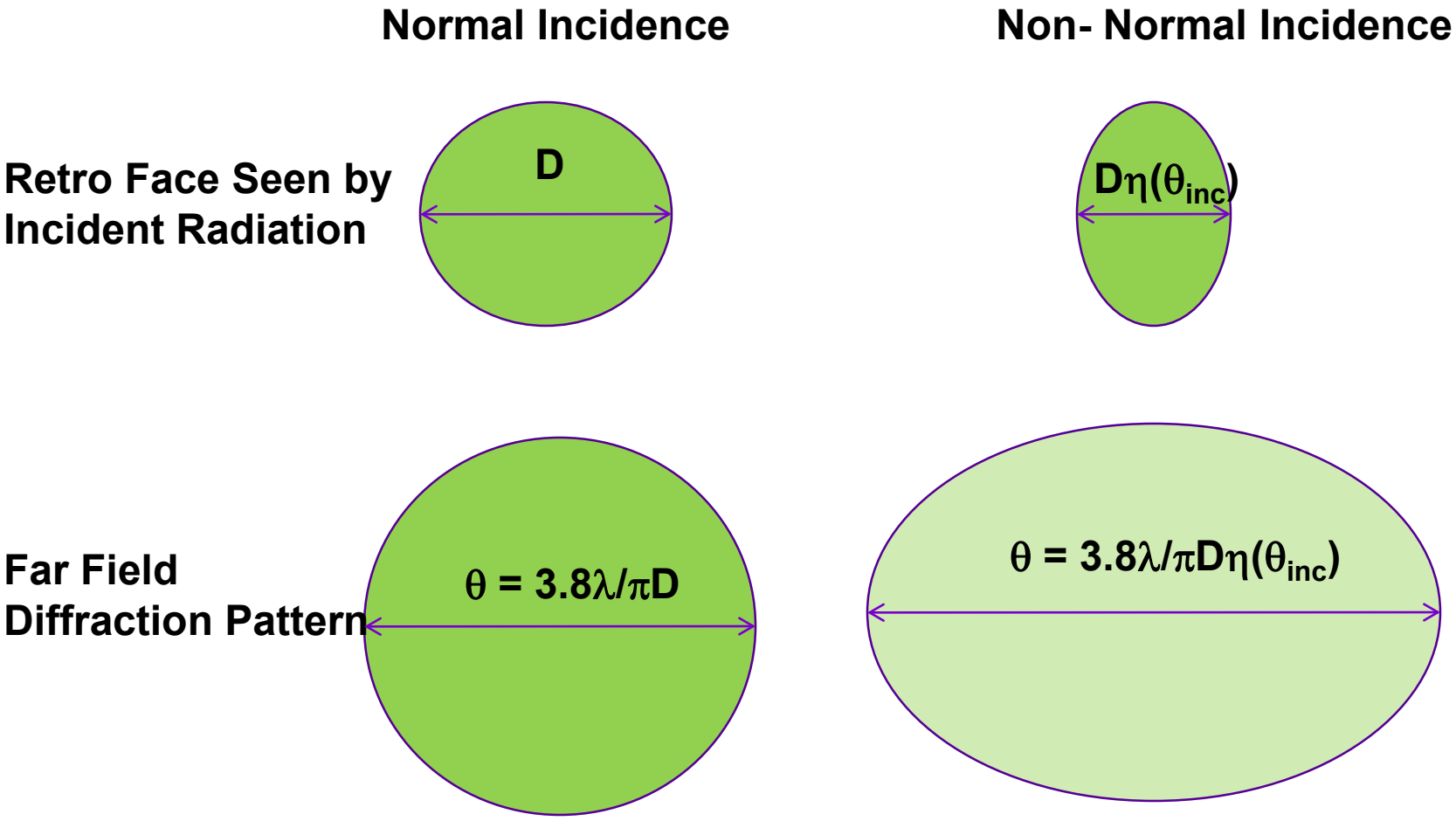

Starlette and LAGEOS*

Since, for maximum accuracy orbit determination, the distance of the effective light reflection point from the satellite center of mass is ideally independent of the viewing angle, geodetic satellites are typically spheres embedded with retros. Furthermore, since the signal strength decreases with satellite range as $1/R^4$, the sphere diameter is increased to accommodate more retros and meet cross-section (signal strength) requirements.

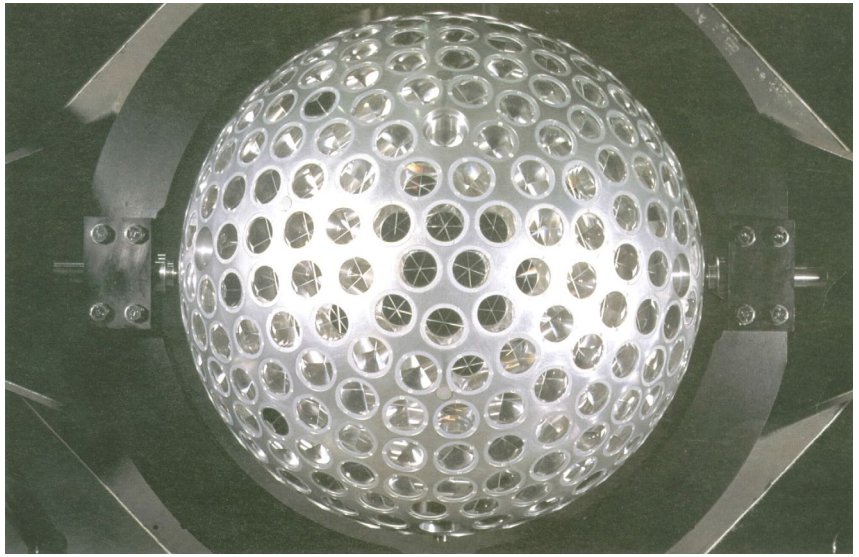

Starlette
CNES, France
Launch: 1975
Diameter: 24 cm
Number of Retros: 60

LAGEOS
NASA, USA
Launch: 1976
Diameter: 60 cm
Number of Retros: 426 (4 Ge for NIR)

* LAGEOS-2 (Italy) was launched from the NASA Space Shuttle in 1992.

Satellite Contribution to the Range Variance

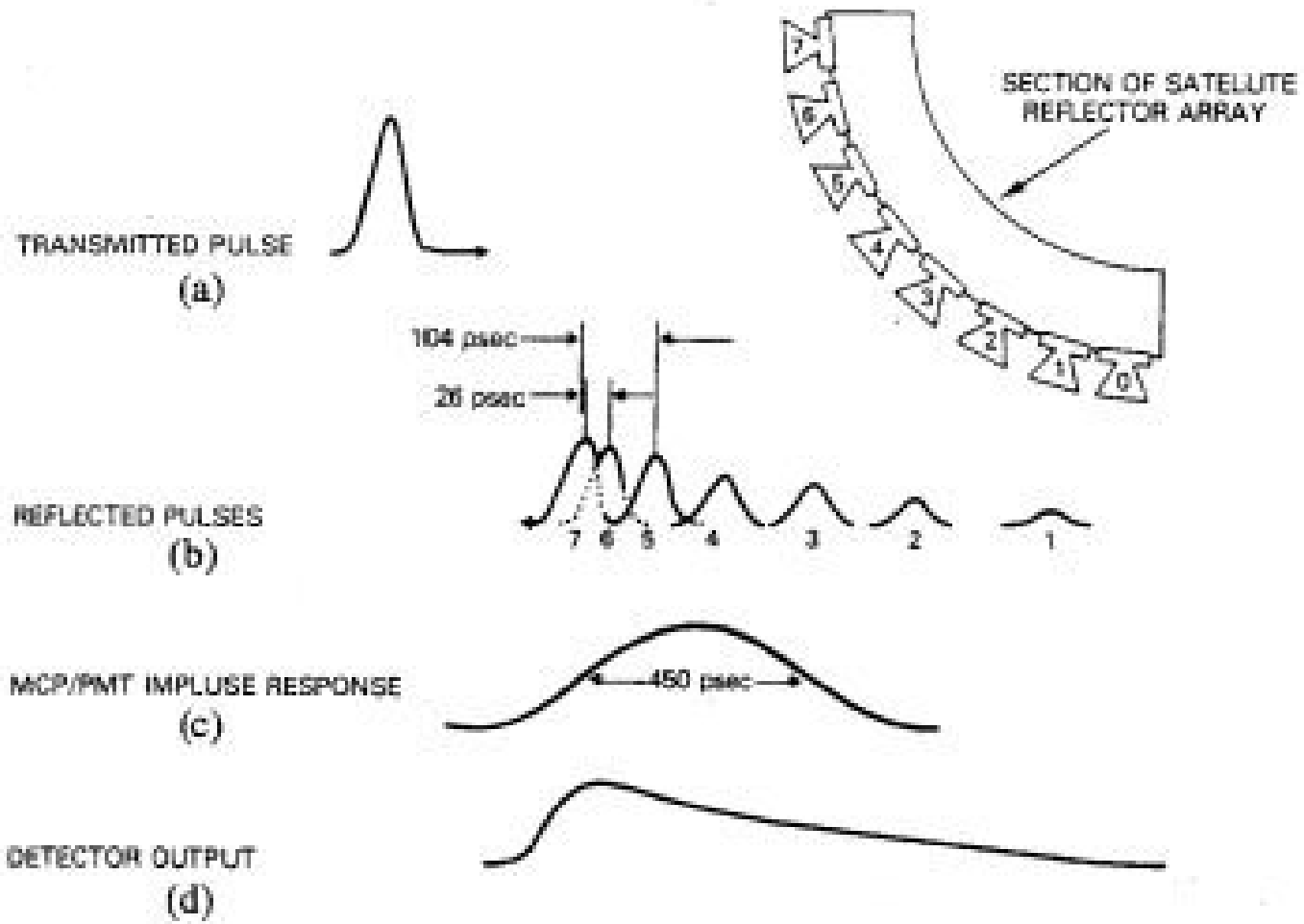

Fig. 9. LAGEOS induced pulse spreading.

Note that the satellite impulse response (range variance) will vary slightly depending on where the line of sight between the station and the satellite CoM falls within the array.

In the following graph, τ is a time normalized to the time it takes a light pulse to travel the diameter of the satellite, i.e. $2R_s/c$. Increasing the radius of the satellite to make it appear flatter will increase the cross-section but broaden the impulse response. However, narrowing the incidence angle response by using hollow cubes or recessing the solid cubes reduces the width of the satellite impulse response (range variance) and improves range accuracy. However, on the positive side, the larger satellite radius increases the number of retros illuminated by the laser and hence the effective cross-section and received signal strength.

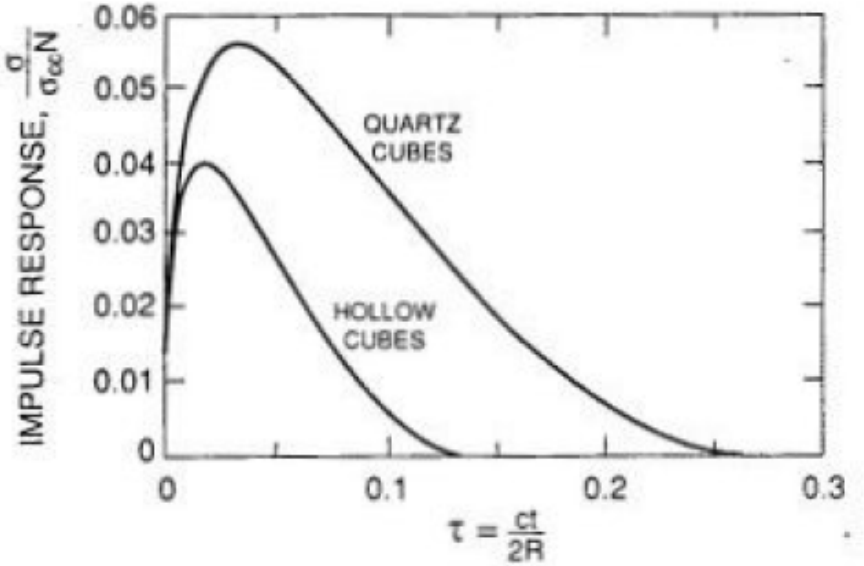

Fig. 27. Impulse response in the large satellite limit ($R_s \gg nL$) for both hollow and solid quartz cube corners.

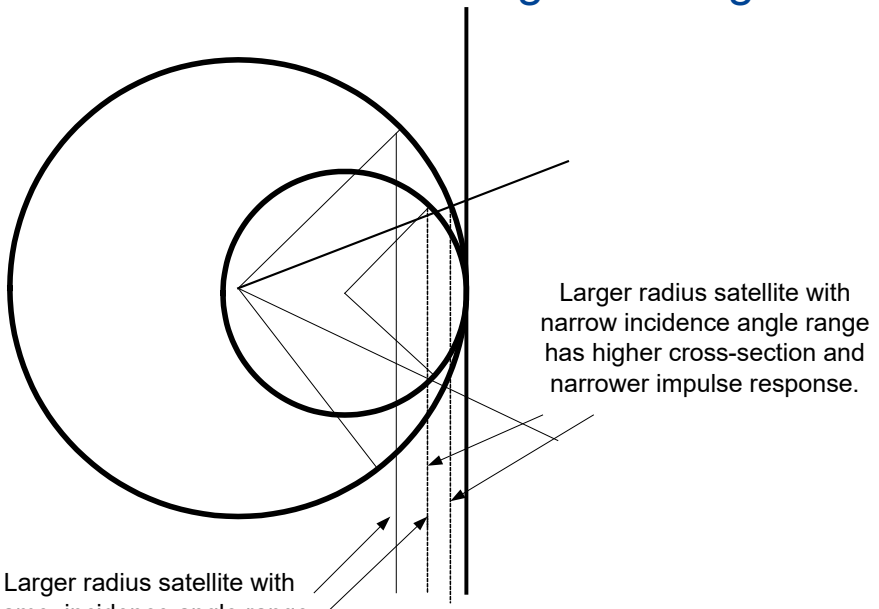

SLR Missions and Orbits

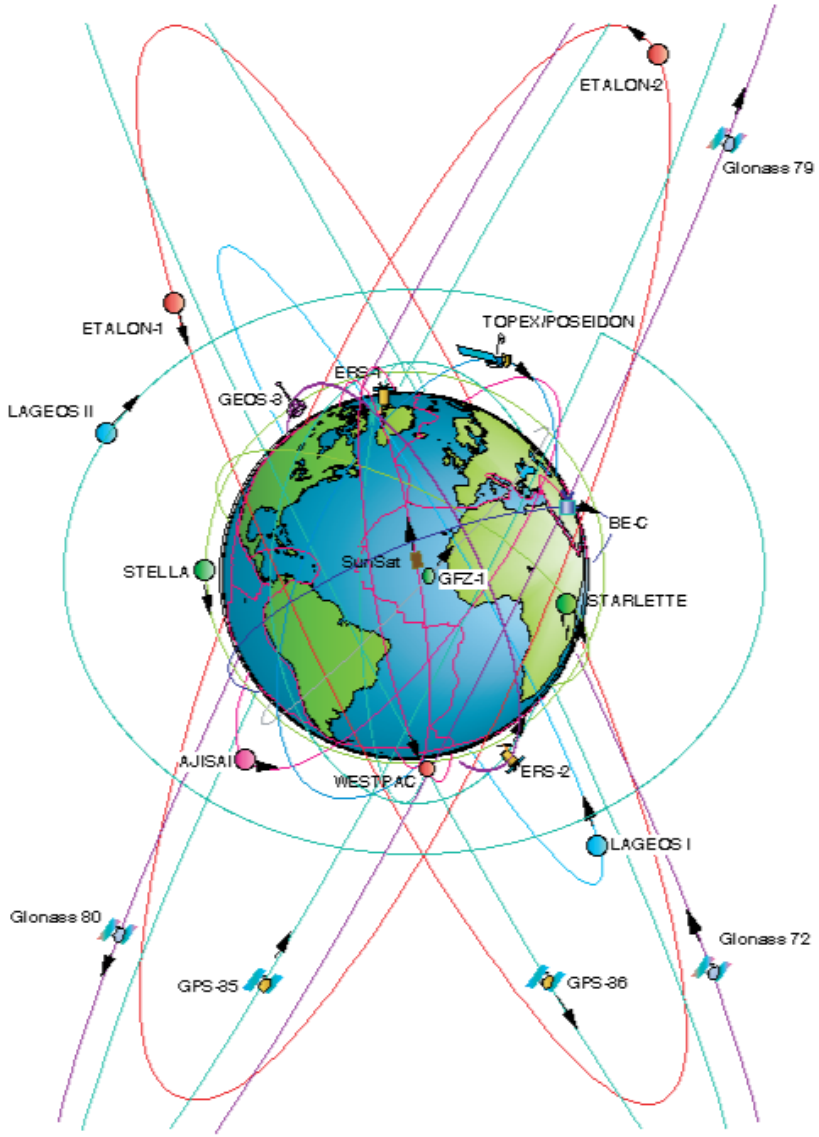

The current SLR constellation spans a wide range of altitudes (500 km to 36,000 km) and inclinations and each retroreflector array has to be designed accordingly based on orbital altitude, mission goals, desired signal strength, etc. The satellites typically fall into four altitude realms with very different science goals:

1. Low Earth Orbiting (LEO: h<1,500 km)
   - Higher Order Gravity Field Studies
   - Spaceborne Radar/Lidar Orbital Support for observing terrain, sea/ice levels, etc.
2. Medium Earth Orbiting (MEO: h~6,000 km)
   - Low drag MEO satellites such as LAGEOS 1 and 2 are ideal for observing relative station positions, tectonic plate motion, regional crustal deformation, etc.
3. Global Navigation System Satellites (GNSS: h~20,000 km)
   - SLR provides Orbital support to International Navigation Constellations such as GPS (US), GLONASS(Russia), GALILEO (EU), COMPASS/BeiDou (China), etc and enhances the accuracy of GNSS orbits and ground networks
4. Geosynchronous (GEO: h ~36,000 km)

Velocity Aberration

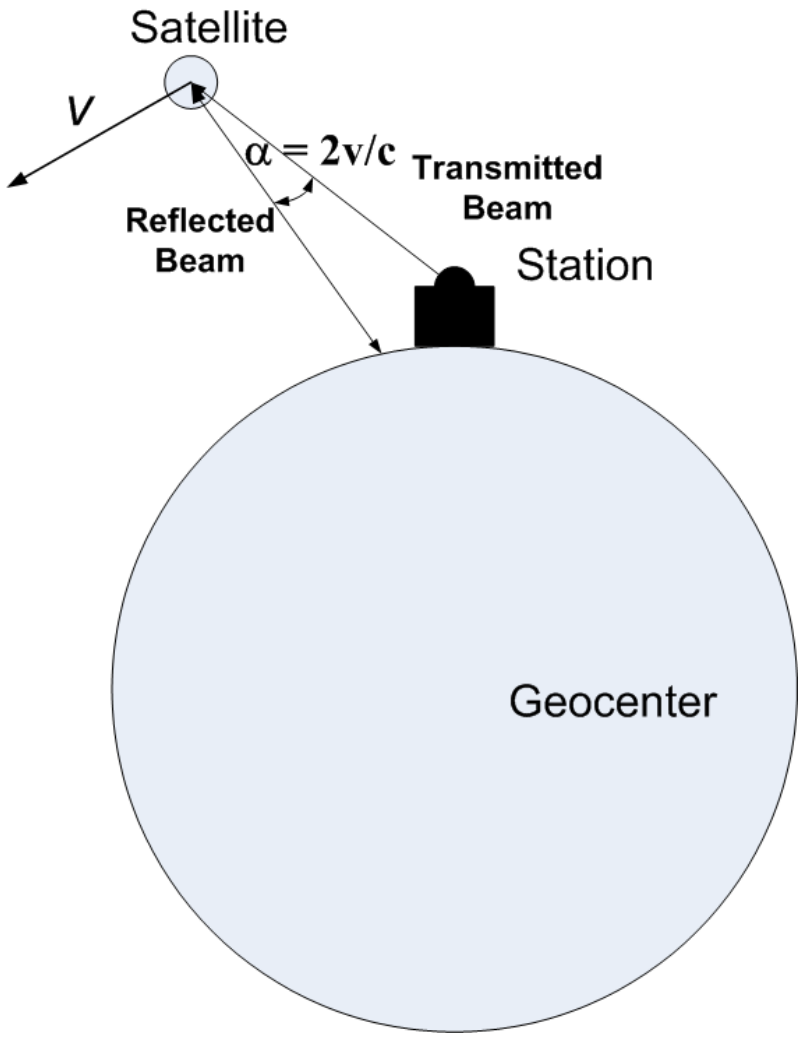

•If there is no relative velocity between the station and satellite, the beam reflected by the retroreflector will fall directly back onto the station .

• However, a relative velocity, v, between the satellite and station causes the reflected beam to be angularly deflected from the station in the forward direction of the satellite motion by an angle $\alpha = 2v/c$ where c is the speed of light.

•Since small diameter cubes have small optical cross-sections but large angle FFDPs , the signal at the station is not significantly reduced by velocity aberration.

•On the other hand, large diameter cubes with high cross-sections have small angle FFDPs, and the signal at the station is therefore substantially reduced by velocity aberration.

•In general, the signal is reduced by half or more if the cube diameter, D_{cc}, satisfies the inequality

$$D_{cc} > D_{1/2} = \frac{1.6\lambda}{\pi\alpha} = \frac{0.8\lambda c}{\pi v}$$

Velocity Aberration vs Orbital Altitude

J. Degnan, Contributions of Space Geodesy to Geodynamics: Technology, Geodynamics 25, pp. 133- 162 (1993)

If there is a relative velocity between the satellite and the station, the coordinates of the FFDP are translated in the direction of the velocity vector. The magnitude of the angular displacement in the FFDP is given by

$$\alpha(h_s,\theta_{zen},\omega)=\alpha_{\max}(h_s)\sqrt{\cos^2\omega+\Gamma^2(h_s,\theta_{zen})\sin^2\omega}$$

where the maximum and minimum values are given by

$$\alpha_{\max}(h_s)=\alpha(h_s,0,0)=\frac{2v_s}{c}=\frac{2}{c}\sqrt{\frac{gR_E^2}{R_E+h_s}}$$

Red line in graph

$$\alpha_{\min}(h_s)=\alpha(h_s,70^o,90^o)=\alpha_{\max}(h_s)\Gamma(h_s,70^o)$$

Blue line in graph

$$\Gamma(h_s,\theta_{zen})=\sqrt{1-\left(\frac{R_E\sin\theta_{zen}}{R_E+h_s}\right)^2}<1$$

$$\omega=\cos^{-1}\left[\left(\hat{r}\,x\,\hat{p}\right)\bullet\hat{v}\right]$$

v_s = satellite velocity at altitude h_s
R_E = Earth radius = 6378 km
g = surface gravity acceleration =9.8m/sec^2
h_s=satellite height above sea level
c = velocity of light = 3x10^8 m/sec
θ_{zen} = largest satellite zenith angle for tracking = 70^o
r = unit vector to satellite from the geocenter
p = unit vector from station to satellite
v= unit vector in direction of satellite velocity

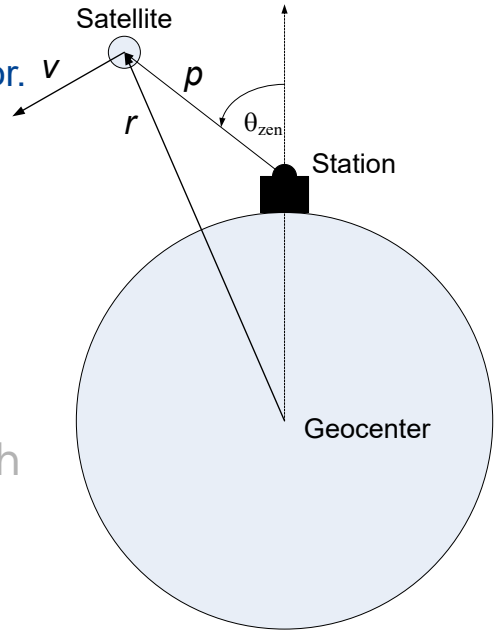

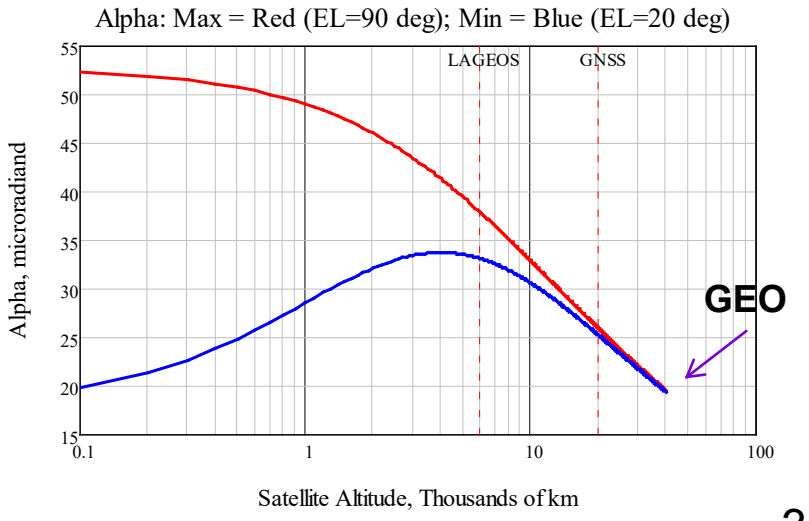

Spoiled Retroreflectors

•"Spoiling" is used to compensate for velocity aberration and improve the signal return from the satellite.

• If we offset one or more (N = 1 to 3) of the cube dihedral angles from 90° by an amount δ, the central lobe of the FFDP splits into 2N spots.

• If n is the cube index of refraction, the mean angular distance of the lobe from the center of the original Airy pattern increases linearly with the dihedral angle offset, δ, according to

$$\gamma = \frac{4}{3}\sqrt{6}n\delta = 3.27n\delta$$

•As before, the angular size of any given lobe decreases as the cube diameter gets larger.

•The FFDP of each lobe is the 2D Fourier transform of an individual 60° sector. The energy distribution is complex but has hexagonal symmetry if all three δs are equal.

•Furthermore, the effective area and peak cross-section of each lobe is reduced to

$$A_{eff} = \eta(\theta_{inc})\frac{A_{cc}}{2N} \qquad \sigma_{peak} = \eta^2(\theta_{inc})\frac{\sigma_{cc}}{(2N)^2}$$

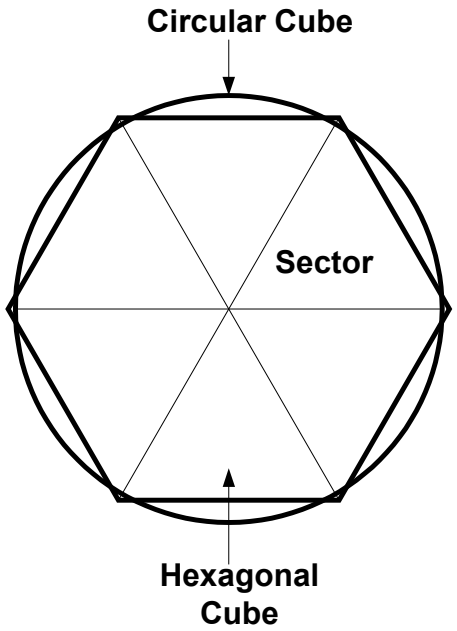

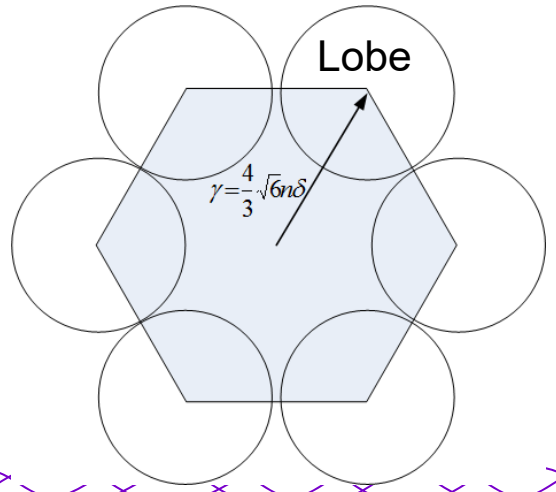

Clocking

Since the return signal is weakest at the lowest elevation tracking angle, choosing $\gamma = \alpha_{min}$ places the peak of the lobe there but any lobe energy inside the inner dark ring is wasted. Filling in circumferential gaps between lobes can be accomplished by rotating adjacent cubes by an angle equal to 60^o divided by an integer greater than 1.·· A smaller lobe diameter will reduce the spillover into the region outside the outermost dark circle but will also create a larger gap between lobes which in turn requires more clocking positions.

0^o Clocking

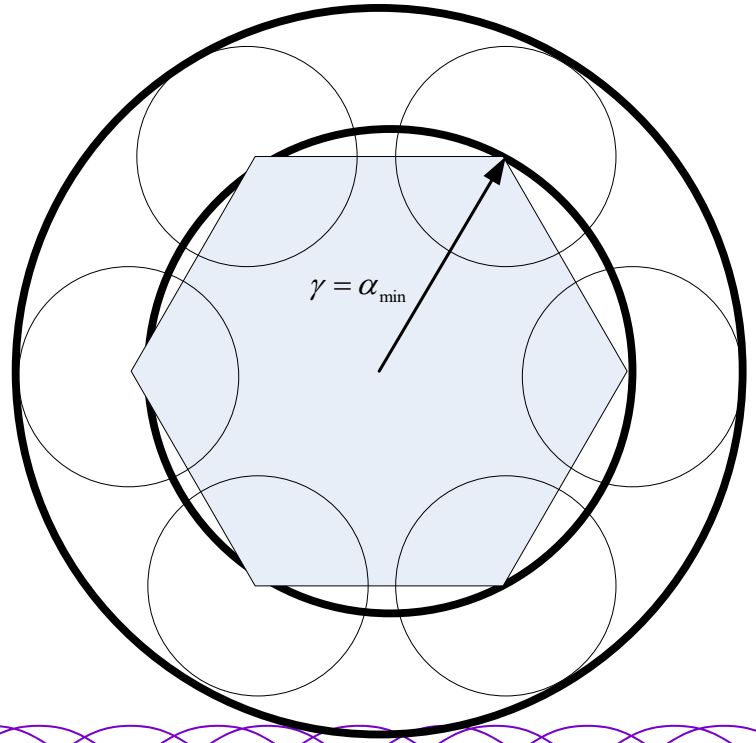

30^o Clocking

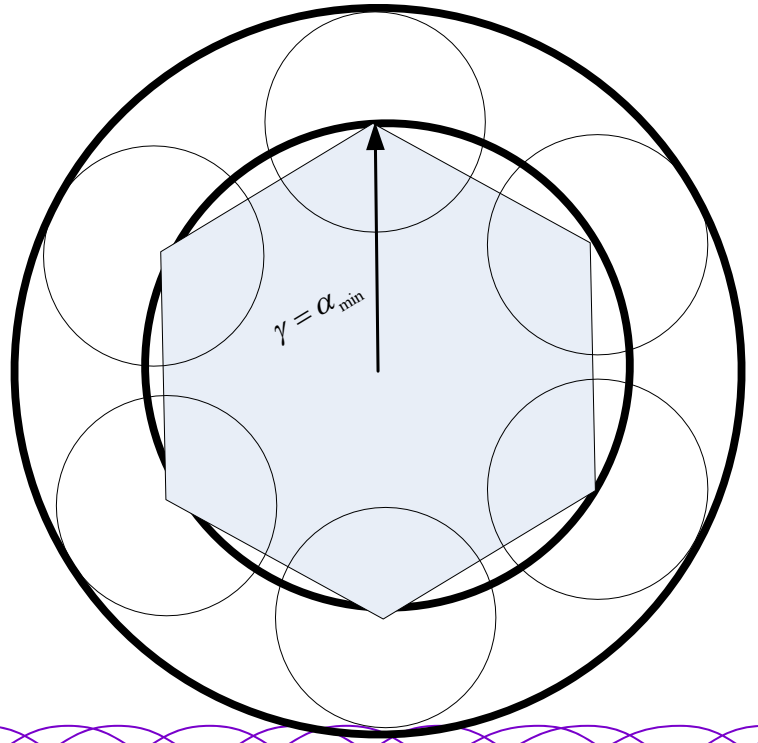

Space Segment Summary

mm Accuracy LEO to MEO Geodetic Satellites

- Use large radius spherical satellites to:
  - better match the incoming plane wave and minimize pulse spreading
  - allow more reflectors within the active area to increase cross-section
- Reduce range of accepted incidence angles to minimize satellite impulse response width via
  - Hollow cubes
  - Recessed hollow or solid cubes
- Also incidence angles < 17° do not leak light in solid TIR reflectors
- Selection of cube diameters and clocking to best match the "α annulus" while favoring the response at high zenith (low elevation) angles is key to efficient array design

GNSS and GEO Satellites

- Typically have a nadir face pointed near Earth center due to other functions (e.g.,Earth observation, communications, navigation, etc.)
- Flat panels OK but still several hundred psecs of temporal spread at low satellite elevation angles. Flat circular (rather than rectangular) arrays would remove azimuthal range biases.
- Range accuracy would further benefit from replacing flat panels by segments of a large sphere

LLR

- Characterized by small incidence angles (<1 deg ignoring lunar librations) and velocity aberrations (<1.0 arcsec) suggest the possible use of large diameter cubes provided thermal issues on the lunar surface can be resolved.

Observing Satellite Rotation with Single Photons

Courtesy: Georg Kirchner, Graz SLR, Austria

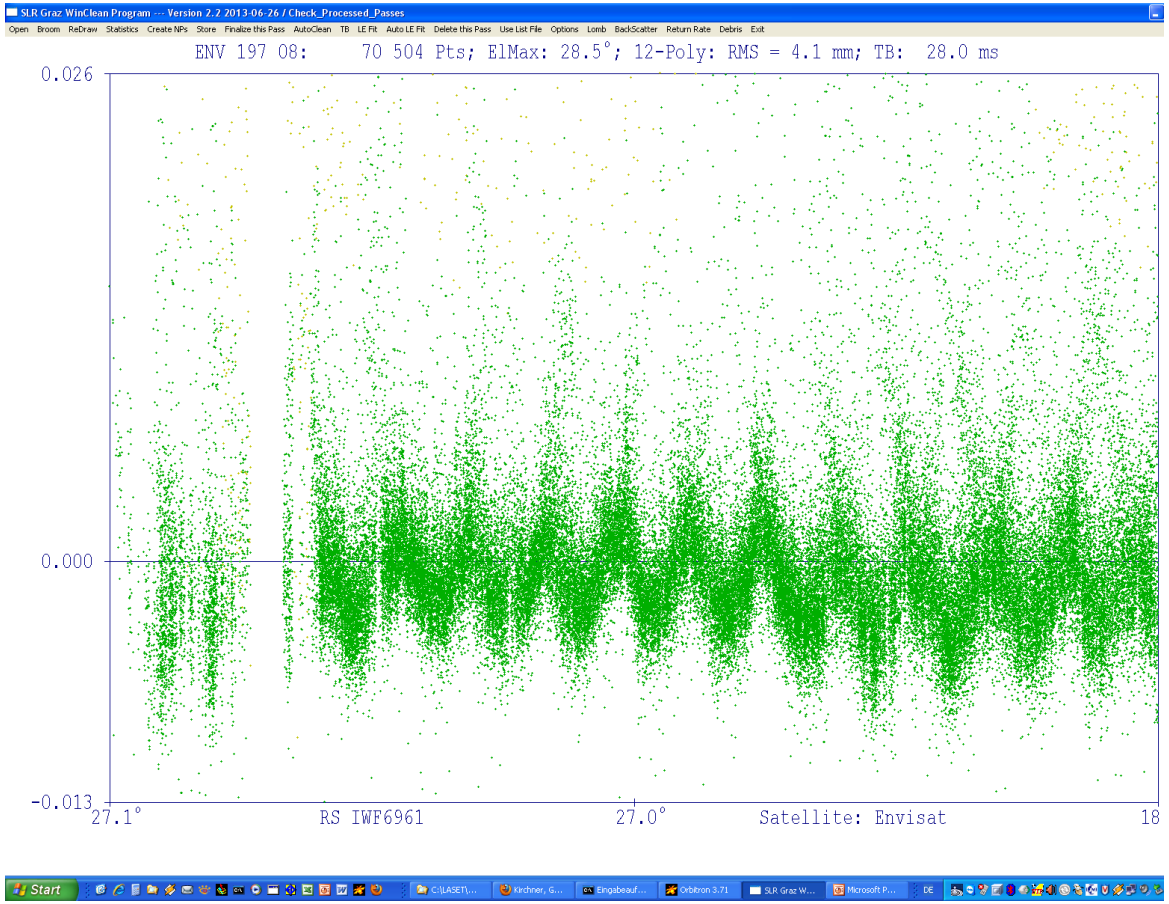

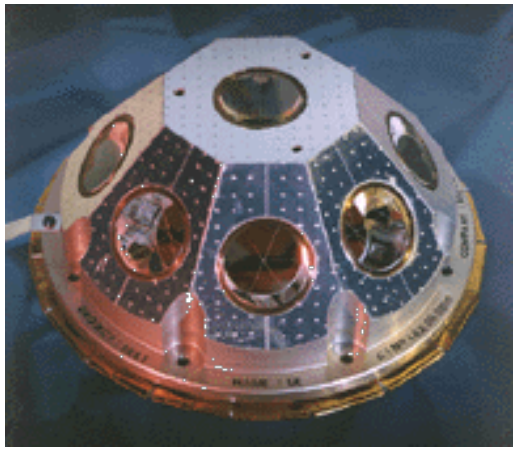

ENVISAT Retro Array

Graz Laser Characteristics:
Energy: 0.4 mJ @ 532 nm
Pulsewidth: <20 psec
Fire Rate: 2 kHz
50 cm receive telescope

Ultra short pulses at kHz rates greatly increase temporal and spatial (range) resolution and allow one to see individual retroreflectors as the satellite rotates.

Laser Debris Ranging 2013

Courtesy: Georg Kirchner, Graz, Austria

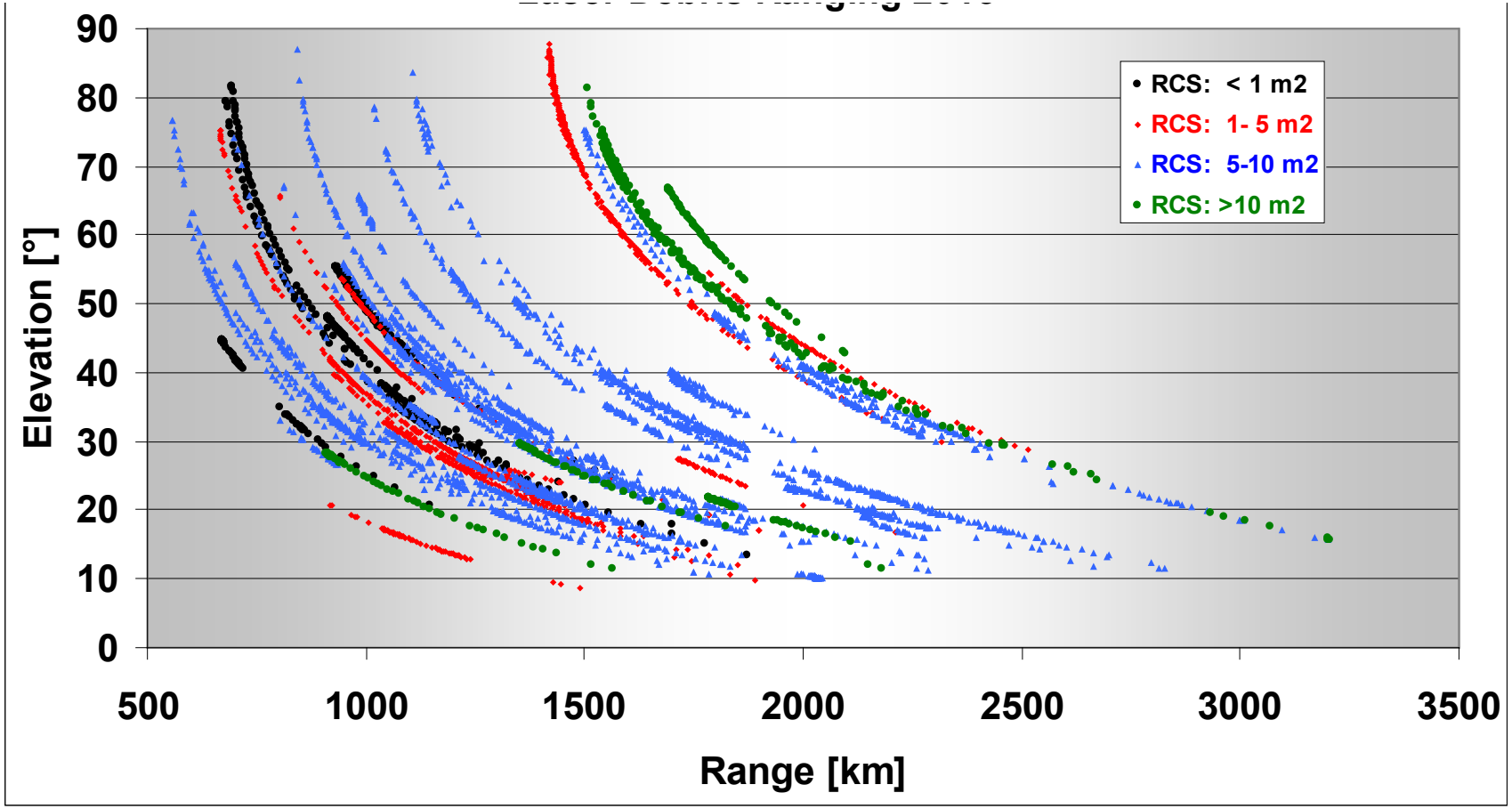

2013: In 13 Sessions – each about 2 to 3 h during early evening - >200 passes of about 60 objects measured; up to 3000 km distance . RCS = Radial Cross Section.
Pulse Energy: 200 mJ; Pulsewidth: 3 nsec; Fire Rate: 80 Hz. Flashlamp-pumped.

EUROPEAN MULTISTATIC EXPERIMENT

Courtesy: Georg Kirchner, Graz, Austria

Graphics: © Peter Ruzek / AIUB

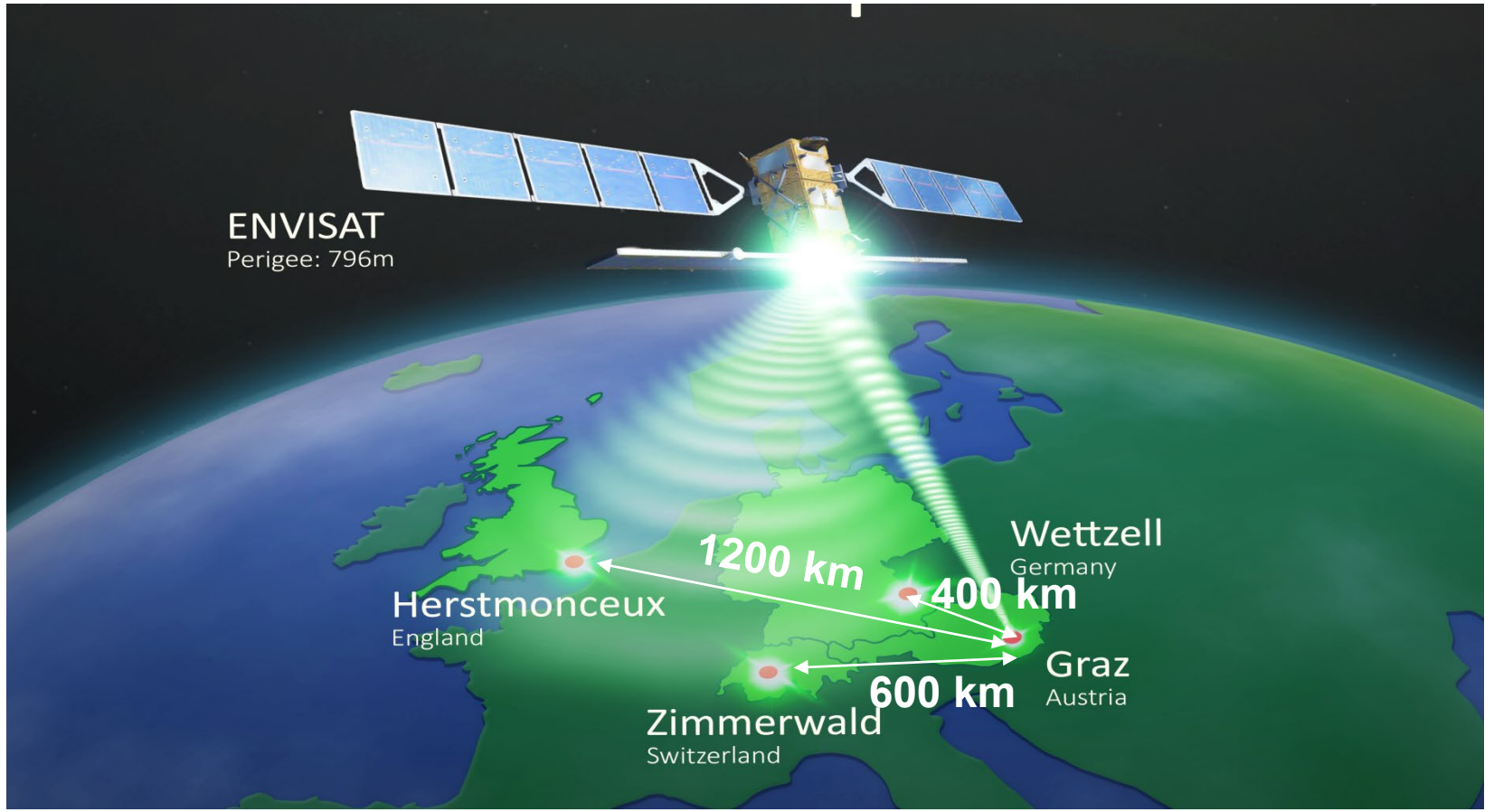

SATELLITE LASER RANGING WITHOUT RETROREFLECTORS!

ONE active station (Graz) fires high energy laser pulses at a satellite with no retroreflectors. The laser photons are reflected diffusely from the satellite and the weak reflections are detected and timed at several distant passive stations equipped with single photon sensitive detectors.

Austrian Photons off Space Debris Detected in Germany
Courtesy: Georg Kirchner, Graz SLR

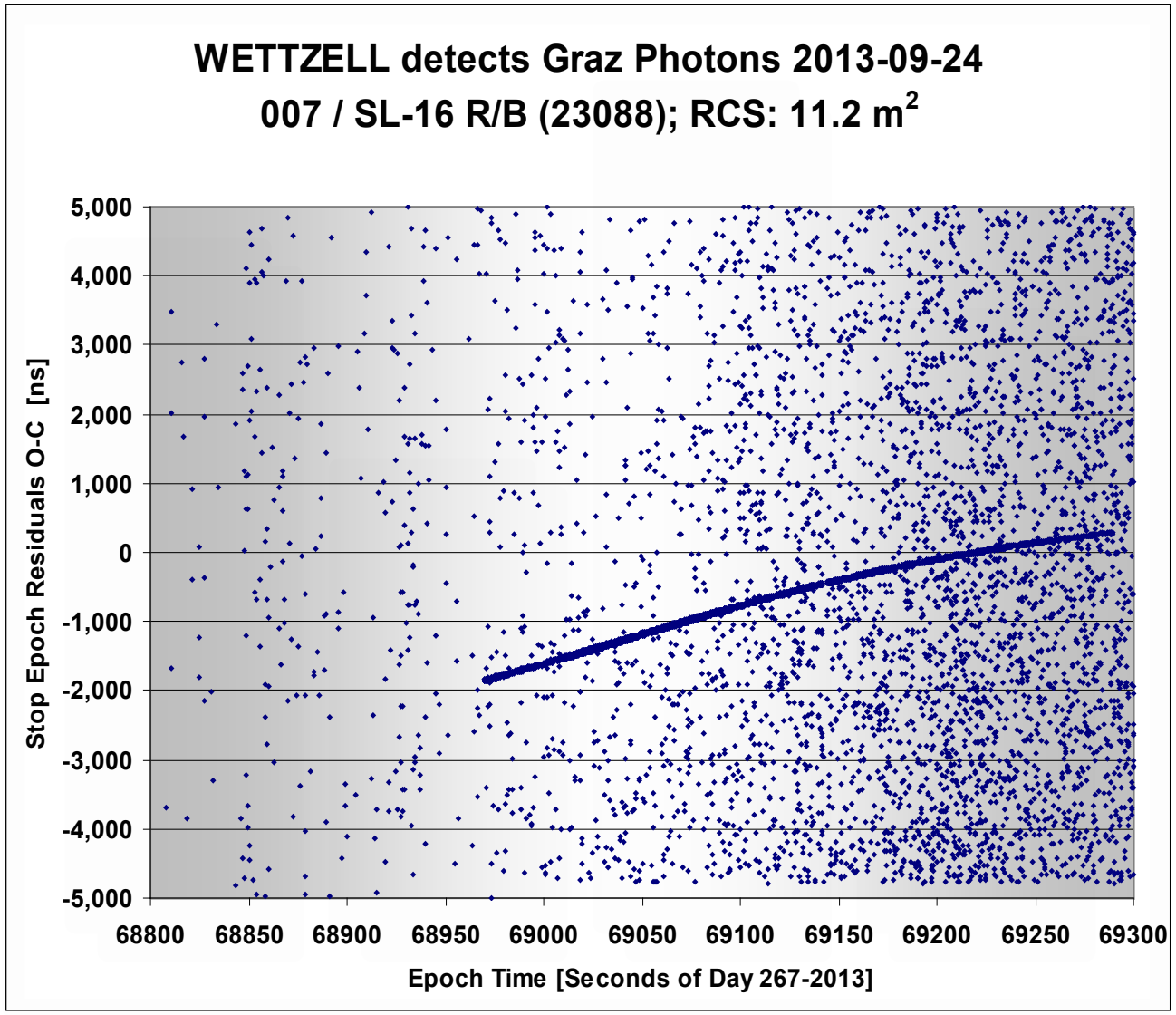

- Example: Graz fires to an old rocket body: 11 m² Radar Cross Section (RCS)

- Photons are reflected diffusely and detected in Wettzell:Clear signal visible …

- Distance: 1800 to 2500 km Elevation: 20° to 10° ↓ (as seen from Graz)

- Debris Laser Firing Rate: 80 Hz

--Maximum Pulse Energy 200 mJ @ 532 nm

-Laser Pulsewidth: 3 nsec

-Flashlamp Pumped

International Laser Ranging Service (ILRS*)

The ILRS was created in 1998, at the urging of Dr. Gerhardt Beutler of Switzerland, by cofounders Dr. John Degnan (NASA Goddard Space Flight Center) and Professor Bob Schutz (Univ. of Texas, Austin).The goal was to better coordinate the international tracking of a rapidly growing number of satellites and provide a better forum for the rapid exchange of data and ideas through international workshops. It is governed by an internationally elected Governing Board with elections every two years. Degnan served as the first GB Chairman from 1998 to 2002.

"*The International Laser Ranging Service (ILRS) provides global satellite and lunar laser ranging data and their related products to support geodetic and geophysical research activities as well as IERS products important to the maintenance of an accurate International Terrestrial Reference Frame (ITRF). The service develops the necessary global standards/specifications and encourages international adherence to its conventions. The ILRS is one of the space geodetic services of the International Association of Geodesy (IAG). The ILRS collects, merges, archives and distributes Satellite Laser Ranging (SLR) and Lunar Laser Ranging (LLR) observation data sets of sufficient accuracy to satisfy the objectives of a wide range of scientific, engineering, and operational applications and experimentation. These data sets are used by the ILRS to generate a number of scientific and operational data products* "

*Ilrs.gsfc.nasa.gov

Current ILRS Network

Lunar Laser Ranging

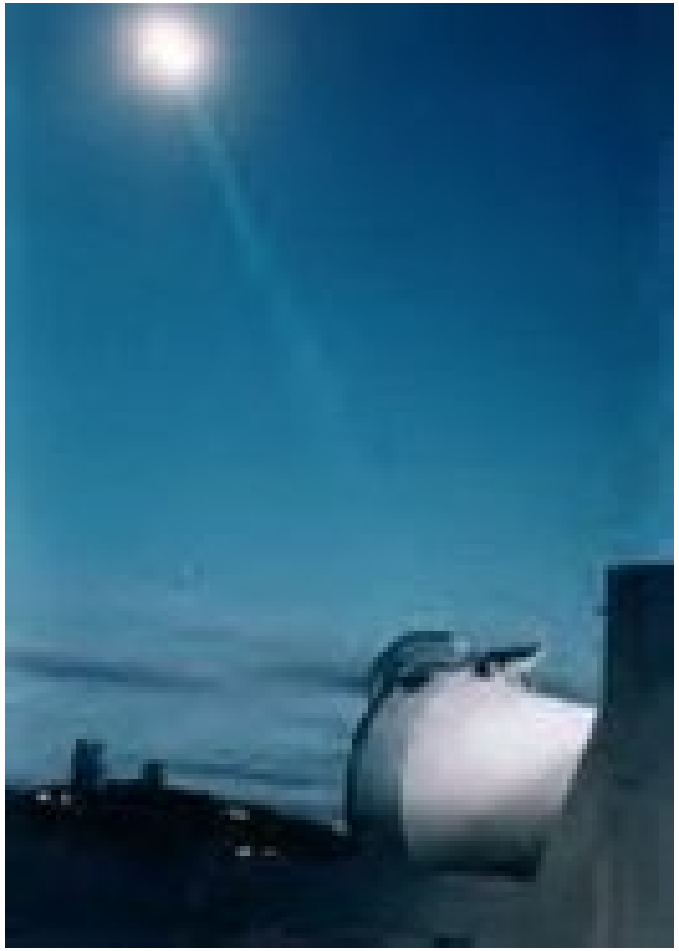

MLRS ranging to the Moon

- Currently five passive retroreflector arrays were landed on the Moon by
  - 3 NASA manned Apollo missions (11,14, and 15)
  - 2 Soviet Lunakhod missions (1 and 2)
- For over 30 years, the LLR data set was provided by three sites:
  - MLRS, McDonald Observatory, Texas, USA
  - CERGA LLR, Grasse, France
  - Mt. Haleakala, Hawaii, USA (decommissioned in 1992)
- New LLR systems have since come online:
  - MLRO, Matera, Italy
  - Apollo, Apache Point, New Mexico, USA (multiphoton, 3.5 m telescope)

Lunar Retroreflector Arrays

Five retroreflector arrays were placed on the lunar surface beginning with Apollo 11 in 1969. Two other manned Apollo missions (14 and 15) also left arrays with Apollo 15 being the largest (300 vs 100 cubes) to strengthen the return signal. Two unmanned Soviet Lunakhod (17 and 21) missions landed additional arrays provided by France. Because the Moon is so far away and maintains a fairly constant angular orientation with respect to the Earth, flat reflector panels could be used.

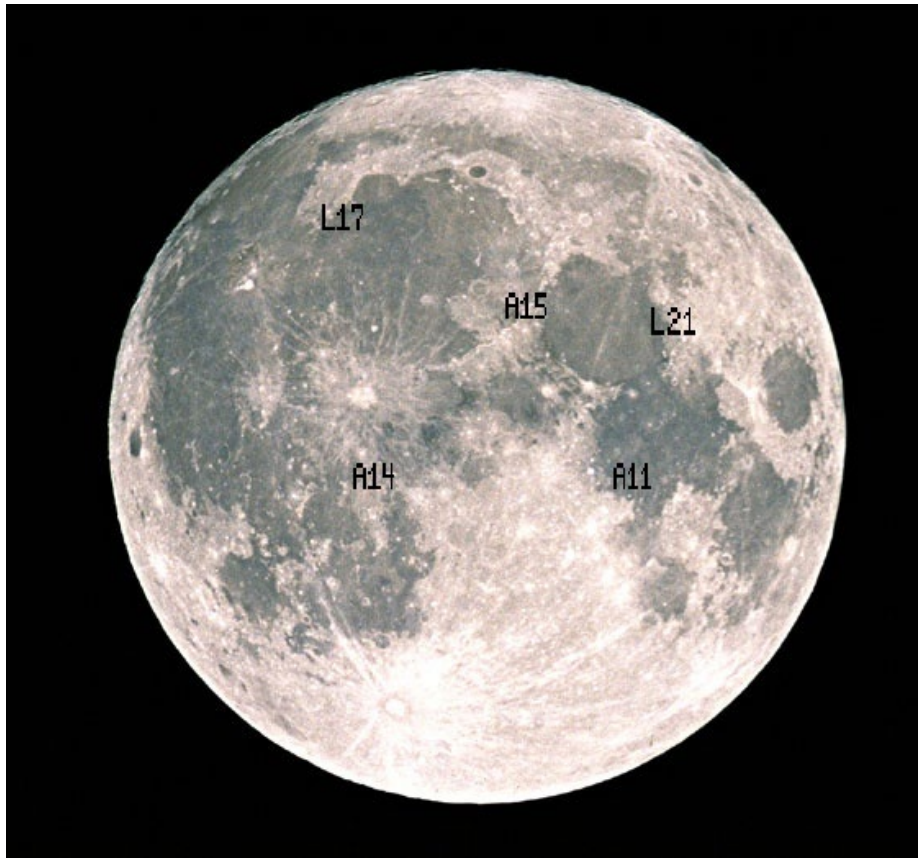

Retroreflector Array Sites

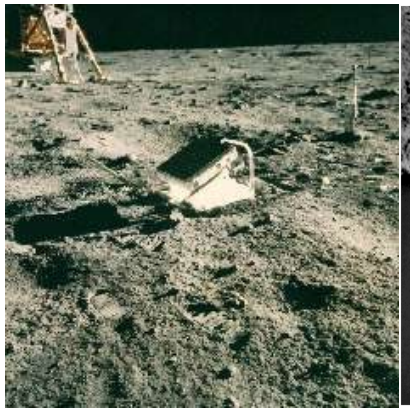

Apollo 11, 1969

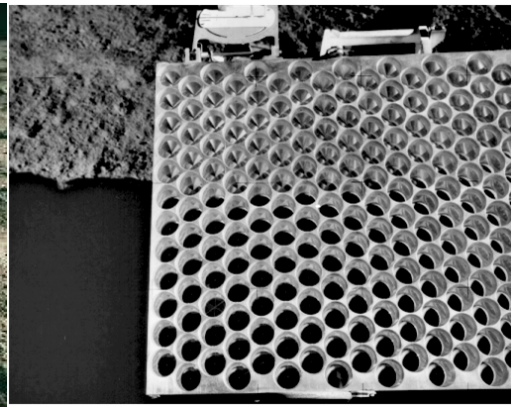

Apollo 15

Array

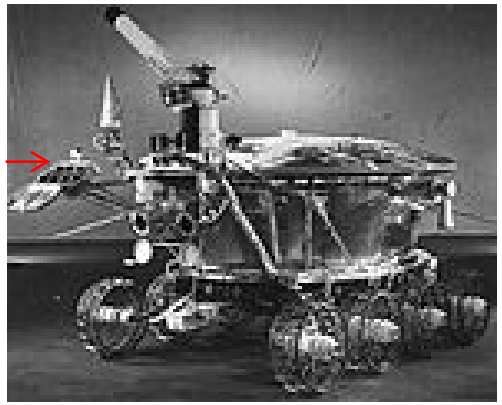

Lunakhod

Apollo 15 Lunar Example

Earth-Moon Distance : $R_{EM} = h+R_E = 384.4 \times 10^6$ m. From the previous equations
α_{max} =6.74 μrad or 1.40 arcsec
α_{min} = 6.68 μrad or 1.39 arcsec at an elevation angle of 20 degrees
v = relative velocity between target and station due to lunar orbital motion = 1km/sec
However, the latter equations ignore the small contribution of station motion due to Earth rotation (~0.46 km/sec) to the relative velocity which typically reduces α to 4 or 5 μrad for LLR but is negligible for LEO to GEO satellites.
If the Apollo reflector arrays are pointed at the center of the Earth, the maximum beam incidence angle on the array from any Earth station (ignoring lunar libration) is

$$\theta_{inc} = a\tan\left(\frac{R_E}{R_{EM}}\right) = 0.95\,\text{deg}$$

The unspoiled cube diameter for which the cross-section falls to half its peak value is

$$D_{1/2} = 40.6mm = 1.6in$$

Typical manufacturing tolerances are 0.5 arcsec for dihedral angles and λ/10 for surface flatness.

Apollo 15 has a flat array of 300 38 mm fused quartz cubes each with an unspoiled peak cross-section of 5.8 x 10^7 m^2. Thus, the theoretical array cross-section, ignoring manufacturing tolerances and local environment effects, is $\Sigma \cong 300(0.5)(5.8 \times 10^7\ m^2) = 8.7 \times 10^9\ m^2$. According to Dave Arnold, polarization losses due to uncoated TIR faces reduce cross-section by factor of 4, leaving $\Sigma \sim 2.2 \times 10^9\ m^2$. The tabulated ILRS value is $1.4 \times 10^9\ m^2$.

Lunar Alternative to Apollo Array

Otsubo et al, Advances in Space Research, Vol. 45, pp. 733-740, 2010.
According to the authors, simulations indicate that a single reflector with a diameter of 150 to 250 mm has similar performance to Apollo arrays. No dihedral angle is required for small diameter reflectors (<150 mm for coated and <100 mm for uncoated and hollow reflectors) . Larger diameters required dihedral angles 0f 0.20, 0.25, and 0.35 arcsec for coated, uncoated, and hollow reflectors respectively.

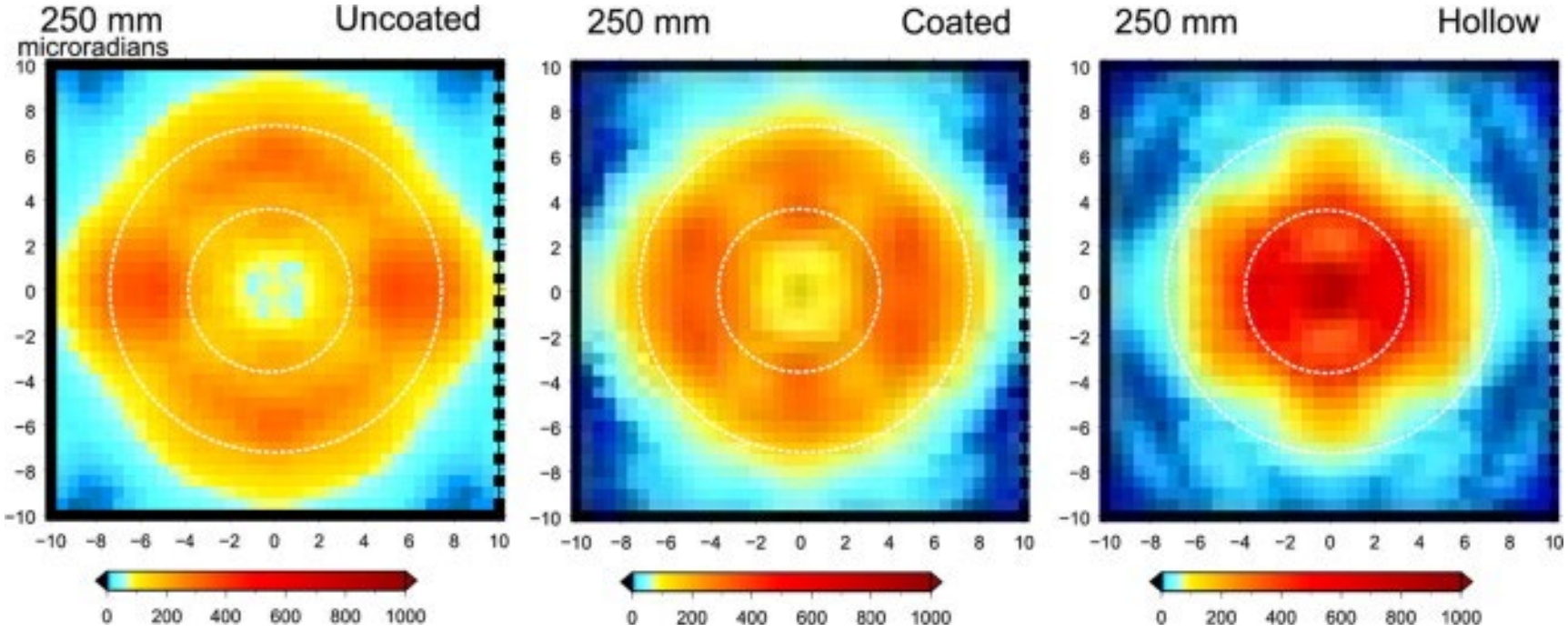

250 mm reflectors with 0.25 arcsec dihedral angles, incidence angle = 6 degrees

LLR Range Precision vs Time

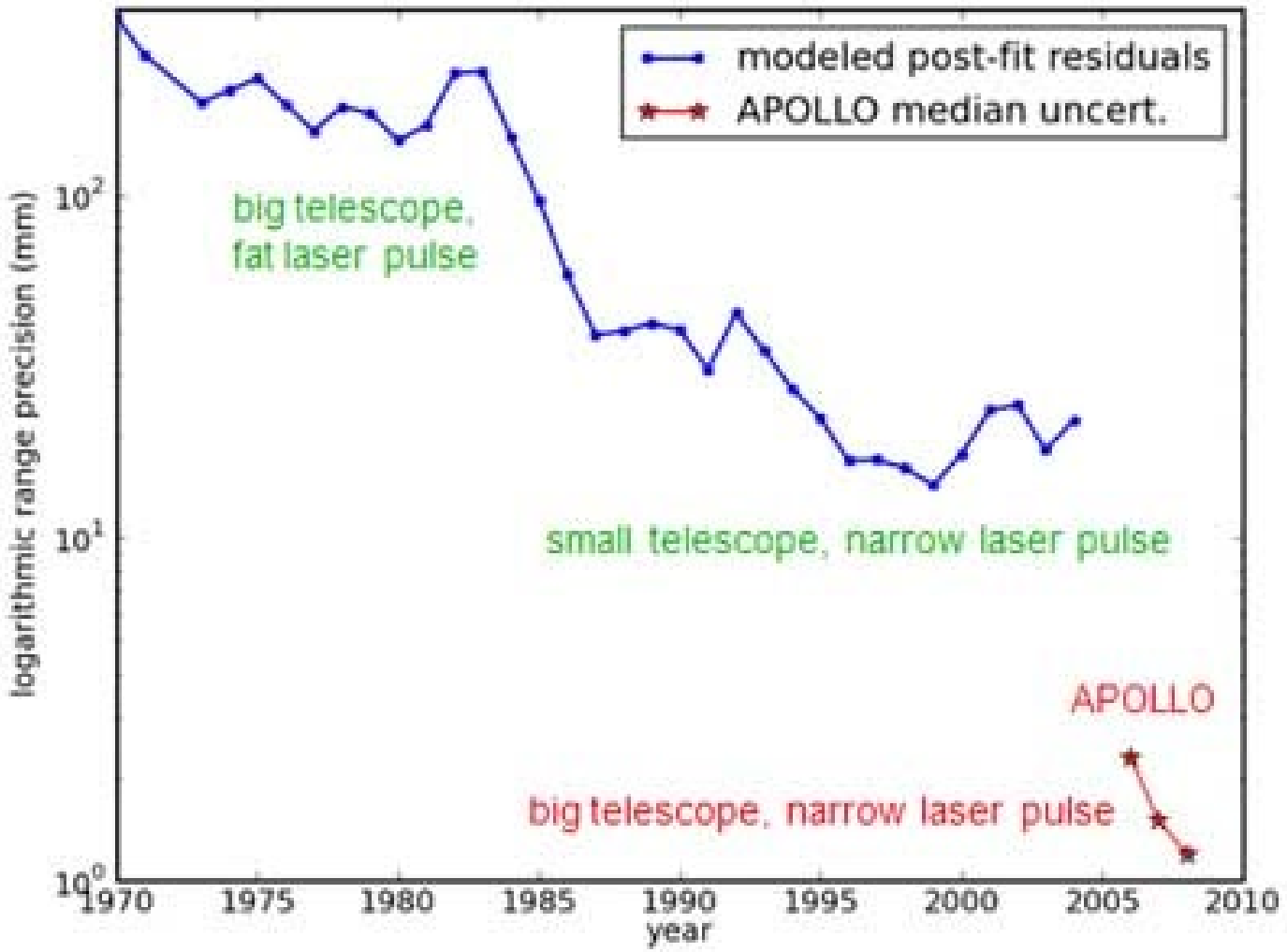

Some LLR Applications

- Lunar Physics
  - Centimeter accuracy lunar ephemerides
  - Lunar librations (variations from uniform rotation)
  - Lunar tidal displacements
  - Lunar mass distribution
  - Secular deceleration due to tidal dissipation in Earth's oceans
  - Measurement of $G(M_E + M_M)$
- Solar System Reference Frame
  - Dynamic equinox
  - Obliquity of the Ecliptic
  - Precession constant
- General Relativity/Fundamental Physics
  - Test/evaluate competing gravitational and relativistic theories
  - LLR validates Einstein's Strong Equivalence Principle (SEP), which states that an object's movement in a gravitational field does not depend on its mass or composition.
  - Constrain β parameter in the Robertson-Walker Metric
  - Constrain time rate of change in G (G-dot)

Laser Applications Beyond the Moon

- Given the current difficulty of laser ranging to passive reflectors on the Moon, conventional single-ended ranging to passive reflectors at the planets is unrealistic due to the R^{-4} signal loss in the link equation.
- Since double-ended laser transponders have active transmitters on both ends of the link, signal strength at either terminal falls off only as R^{-2} and precise interplanetary ranging, time transfer, and communications is possible. Furthermore, since most of the link burden (laser power, telescope aperture) can be carried by the Earth station, the space terminal can be relatively modest in size, weight, and power consumption.

Asynchronous Interplanetary Laser Transponders

*J. Degnan, J. Geodynamics, 34, pp. 551-594 (2002).

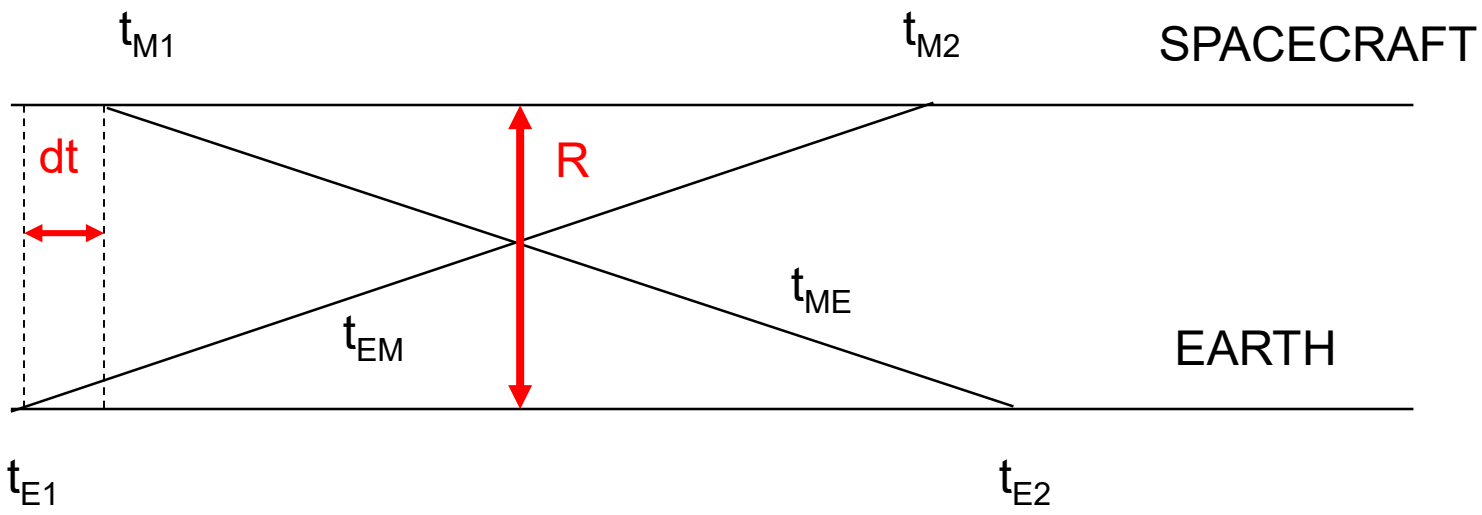

Range $R = c(t_{ME} + t_{EM})/2 = c\,[(t_{E2}-t_{E1})+(t_{M2}-t_{M1})]/2$

Clock Offset $dt = [(t_{E2}-t_{E1})-(t_{M2}-t_{M1})]/[2(1+\dot{R}/c)]$

Laser vs Microwave Links

- **Laser Advantages**
  - Ranging/timing instrumentation is more precise (~1 mm) due to availability of picosecond transmitters, detectors, and timers in the optical regime
  - Divergence of transmitted optical beam is 4-5 orders of magnitude smaller than microwaves for a given transmit aperture (~λ/D) implying
    - More energy captured at the opposite receiver
    - Smaller antennas (telescopes) and transmitters, more lightweight, less prime power
  - Charged particles cannot follow optical frequencies so
    - no propagation delays due to Earth's ionosphere or the interplanetary solar plasma
  - As shown previously, optical atmospheric propagation delay uncertainties are typically at the sub-mm level with ground measurements of pressure, temperature, and relative humidity.
- **Laser Disadvantages**
  - Requires more precise pointing knowledge and control but well within SOA especially for interactions between Earth and planets (and/or their moons) which are visible to large telescopes.
  - Link availability affected by weather and clouds but can be > 99% by utilizing several globally distributed ground sites or alternatively three orbiting terminals
  - As with any new technology, lasers have limited demonstrated space heritage, lifetime and reliability compared to more mature microwave transponders but several laser altimeters have already operated for years from Earth, Lunar, Mars, and Mercury orbits.

Note: it took 15 months to download all of the NASA New Horizons data from Pluto via microwave!

Two-Way Transponder Experiment to the Messenger Spacecraft (May/June 2005)*

GSFC 1.2 Meter Telescope

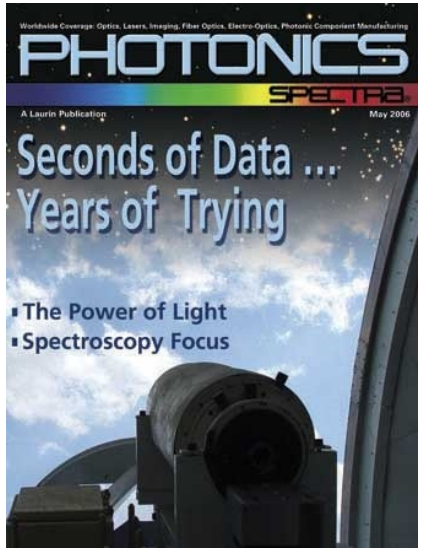

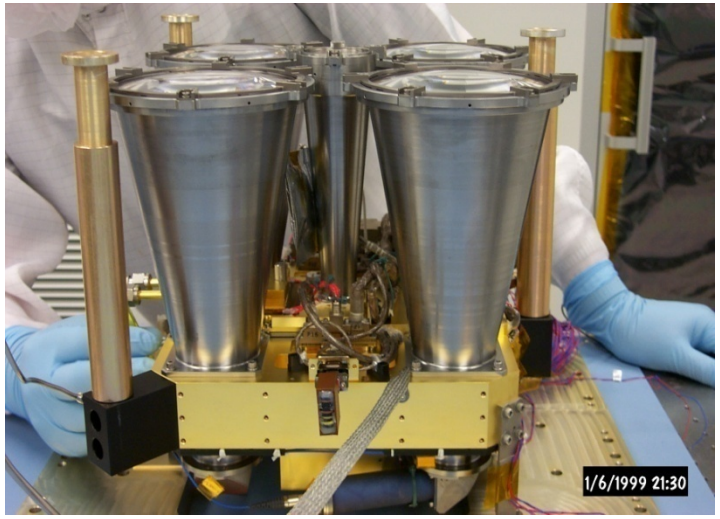

Messenger Laser Altimeter (MLA) enroute to Mercury

24.3 Million Km
20 cm accuracy

*D. E. Smith et al, *Science*, January 2006.

Ground Station
Xiaoli Sun Jan McGarry
Tom Zagwodzki John Degnan
D. Barry Coyle

nce/Analysis/Spacecraft
d Smith Maria Zuber
Neumann John Cavenaugh

One-Way Earth-to-Mars Laser Transponder Experiment (Sept. 2005)

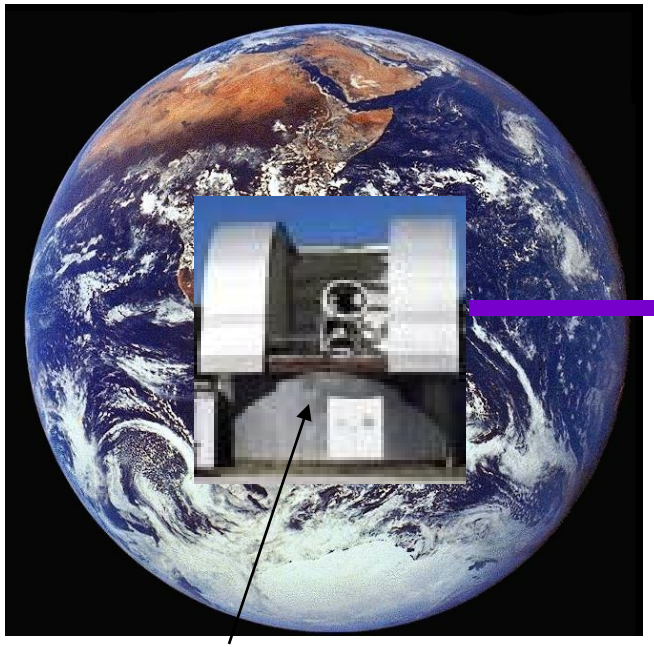

GSFC 1.2 Meter Telescope

80 Million Km!

Mars laser was inoperable but ~500 Earth laser pulses observed at Mars!

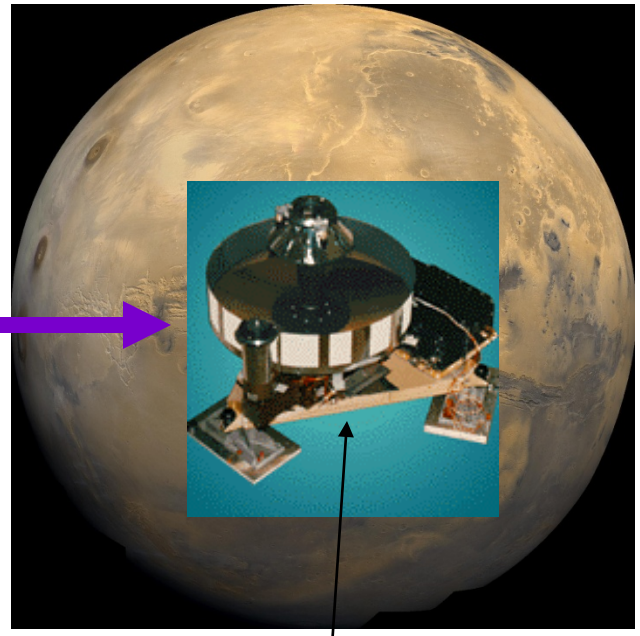

MOLA at Mars

<u>Ground Station</u>

Xiaoli Sun Jan McGarry

Tom Zagwodzki John Degnan

<u>Science/Analysis/Spacecraft</u>

David Smith Maria Zuber

Greg Neumann Jim Abshire

Transponder Link Parameters

*J. Degnan, Int. J. Modern Physics D, 16, pp. 1-14 (2007).

Experiment	MLA (cruise)		MOLA (Mars)
Range (10^6 km)	24.3		~80.0
Wavelength, nm	1064		1064
	Uplink	Downlink	Uplink
Pulsewidth, nsec	10	6	5
Pulse Energy, mJ	16	20	150
Repetition Rate, Hz	240	8	56
Laser Power, W	3.84	0.16	8.4
Full Divergence, μrad	60	100	50
Receive Area, m^2	.042	1.003	0.196
EA-Product, J-m^2	0.00067	0.020	.0294
PA-Product, W-m^2	0.161	0.160	1.64

Table 1: Summary of key instrument parameters for recent deep space transponder experiments at 1064 nm.

Some Transponder Applications

- **Solar System Science**
  - Solar Physics: gravity field, internal mass distribution and rotation
  - Few mm accuracy lunar ephemerides and librations
    - Improves ranging accuracy and temporal sampling over current lunar laser ranging (LLR) operations to Apollo retroreflectors on the Moon with small, low energy, ground stations
  - Decimeter to mm accuracy planetary ephemerides
  - Mass distribution within the asteroid belt
- **General Relativity**
  - Provides more accurate (2 to 3 orders of magnitude) tests of relativity and constraints on its metrics than LLR or microwave radar ranging to the planets, e.g.
    - Precession of Mercury's perihelion
    - Constraints on the magnitude of G-dot ($1x10^{-12}$ from LLR)
    - Gravitational and velocity effects on spacecraft clocks
    - Shapiro Time Delay
- **Lunar and Planetary Mission Operations**
  - Decimeter to mm accuracy spacecraft ranging
  - Calibration/validation/backup for Deep Space Network (DSN) microwave tracking
  - Subnanosecond transfer of GPS time to interplanetary spacecraft for improved synchronization of Earth/spacecraft operations
  - Transponder is a pathfinder technology for interplanetary optical communications and can serve as an independent self-locking beacon for collocated laser communications systems

Part 2: Applications

- Science Contributions of Lunar Laser Ranging (LLR)
  - Earth/Moon Dynamics
  - Tests of General Relativity
- Global Laser Time Transfer
- Using the SLR satellite constellation to simulate interplanetary
  - Ranging
  - Time Transfer
  - Communications
- Satellites Equipped with Microwave or Laser Altimeters
  - Lunar and Planetary Topography
  - Global Sea Level and Ocean Currents
  - Seafloor Topography
  - ICESat-1 and 2
- SLR Earth Science Products
  - Precise Orbit Determination (POD) and Geopotential Model
  - Terrestrial Reference Frame (Center of Mass and Scale)
  - Tectonic Plate Motion and Regional Crustal Deformation
  - Polar Motion and Length of Day

Simulating Interplanetary Ranging, Time Transfer and Communications using the SLR Constellation*

*J. Degnan, Int. J. Modern Physics D, 16, pp. 1-14 (2007).

Transponder Link Equations for Station A (Earth) to Station B (another planet)

Transponder/Lasercom System:

$$n_T^{AB} = \frac{4\eta_q^B \eta_t^A \eta_r^B T_A^{\sec\theta_A} T_B^{\sec\theta_B}}{h\nu_A \left(\theta_t^A\right)^2 (4\pi)} \frac{E_t^A A_r^B}{R_T^2}$$

One/Two-Station Ranging to a Satellite:
One Station implies B = A

$$n_R^{AB} = \frac{4\eta_q^B \eta_t^A \sigma_s \eta_r^B T_A^{2\sec\theta_A}}{h\nu_A \left(\theta_t^A\right)^2 (4\pi)^2} \frac{E_t^A A_r^B}{R_R^4}$$

Setting $n_T^{AB} = n_R^{AB}$ gives us an equivalent transponder range for the two-station SLR experiment

$$R_T(h,\theta_A,\sigma_s) = R_R^2(h,\theta_A)\sqrt{\frac{4\pi}{\sigma_s}\left(\frac{T_B^{\sec\theta_B}}{T_A^{\sec\theta_A}}\right)}$$

$$\cong R_R^2(h,\theta_A)\sqrt{\frac{4\pi}{\sigma_s}\frac{1}{T_A^{\sec\theta_A}}}$$

Simulations can be carried out from either a single SLR station (e.g. Wettzell, Germany) or two adjacent stations (e.g. GSFC 1.2 m and SGSLR in the USA) provided both are located within the far field pattern of the retroreflector array.

Summary of Equivalent Links

- Moon (~0.0026 AU) and Trans-lunar
  - Champ, ERS, Starlette, Jason
- Mercury, Venus, Mars (0.28 to 2.52 AU)
  - LAGEOS (near planetary PCA)
  - Etalon, GPS-35, 36 (Full planetary synodic cycle)
- Jupiter, Saturn, Uranus (4.2 to 18.2 AU)
  - GPS-35, 36 (Jupiter PCA); LRE @25,000 km
- Neptune, Pluto, Kuiper Belt (30 to 50 AU)
  - Future retro-equipped GEO satellites?
- Beyond our Solar System (~100 AU)
  - Apollo 15 lunar array

T2L2 and Compass Time Transfer Experiments

Laser Time Transfer–operational space missions

CTU SPAD photon counters on-board of 5 satellites

China
Compass (Beidou–2) M1
Compass IGSO–1
Compass IGSO–3
Compass M3

T2L2

CNES–NASA
Jason–2, 20. 6. 2008

~100 psec absolute time transfer

LTT package

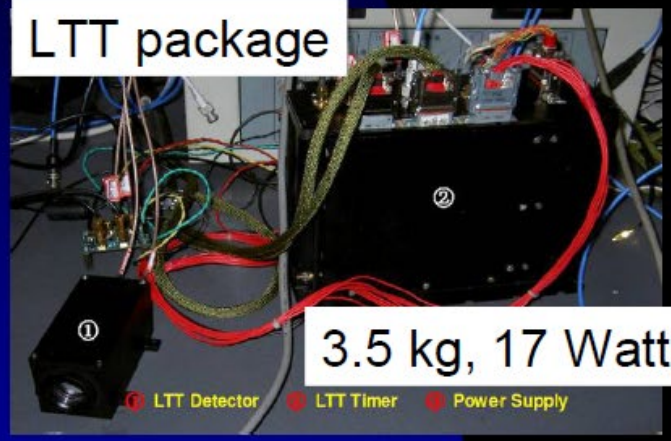

3.5 kg, 17 Watts

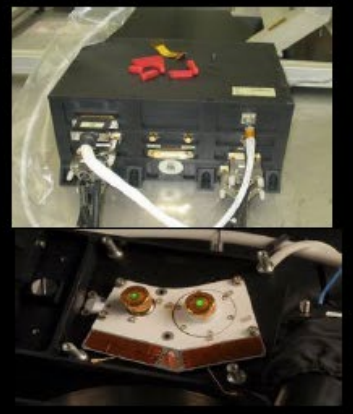

I. Procházka, Praha , červen 2011

Lunar Laser Communications Demonstration (LLCD)

Over the past two decades, there have been several high bandwidth lasercom experiments between Earth-orbiting spacecraft or between spacecraft and a ground station carried out or currently planned by various countries. A low bandwidth link between LOLA/LRO and NGSLR successfully transmitted an image of the Mona Lisa from lunar orbit, but the LLCD on the lunar LADEE mission recently demonstrated a bandwidth of 622 Mbps!

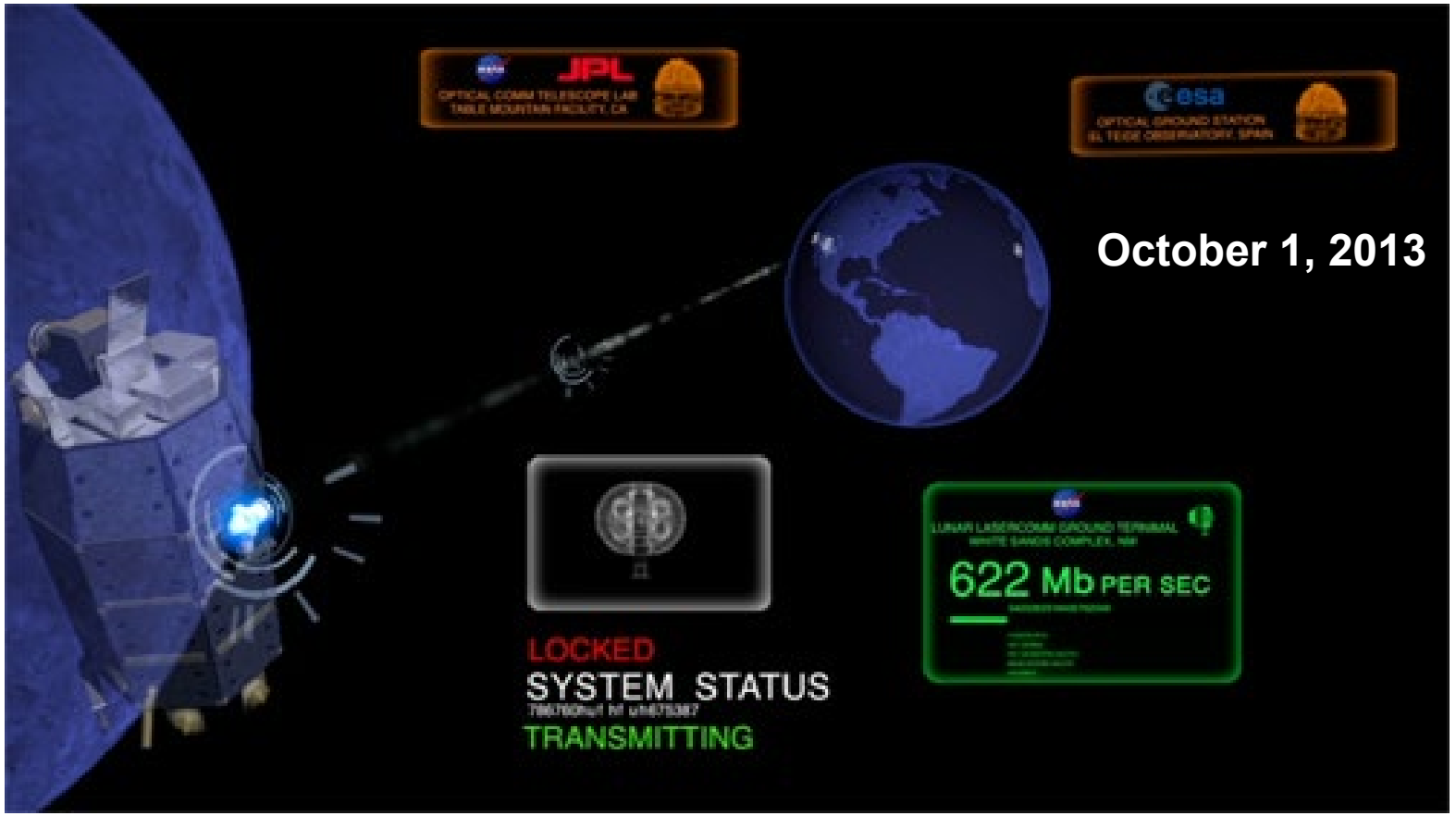

Global Sea Level & Circulation

Radar altimetry on GeoSat, ERS-1, TOPEX/Poseidon, ERS-2, GFO,and JASON satellites, all tracked by SLR

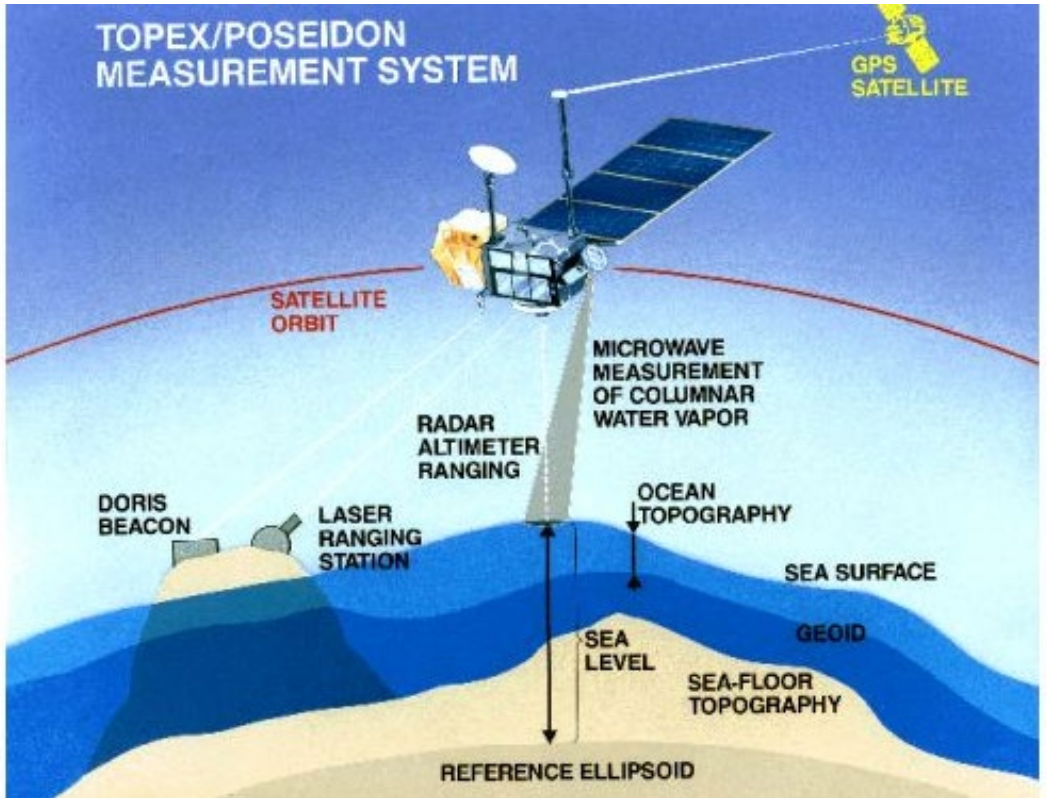

- "Ocean Topography" (OT) is defined as the height difference between the sea surface and the geoid (sum of gravity and Earth rotation effects)
- In the Northern hemisphere, currents flow CW around topographic highs and CCW around lows. The reverse is true in the Southern Hemisphere
- Height of the OT is proportional to the speed of the surface currents.
- Radar (or laser) altimeter measures the distance between the sea surface and the spacecraft on a global scale
- SLR provides:
  - Cm accuracy SLR station locations relative to Geocenter
  - Moderate to long wavelength geoid surface relative to geocenter
  - Cm accuracy positioning of the TOPEX/Poseidon satellite in geocentric reference frame

OT = Satellite Distance from Geocenter (SLR)-Local Geoid (SLR/Alt)-Altimeter Range

Global Mean Sea Level Rise

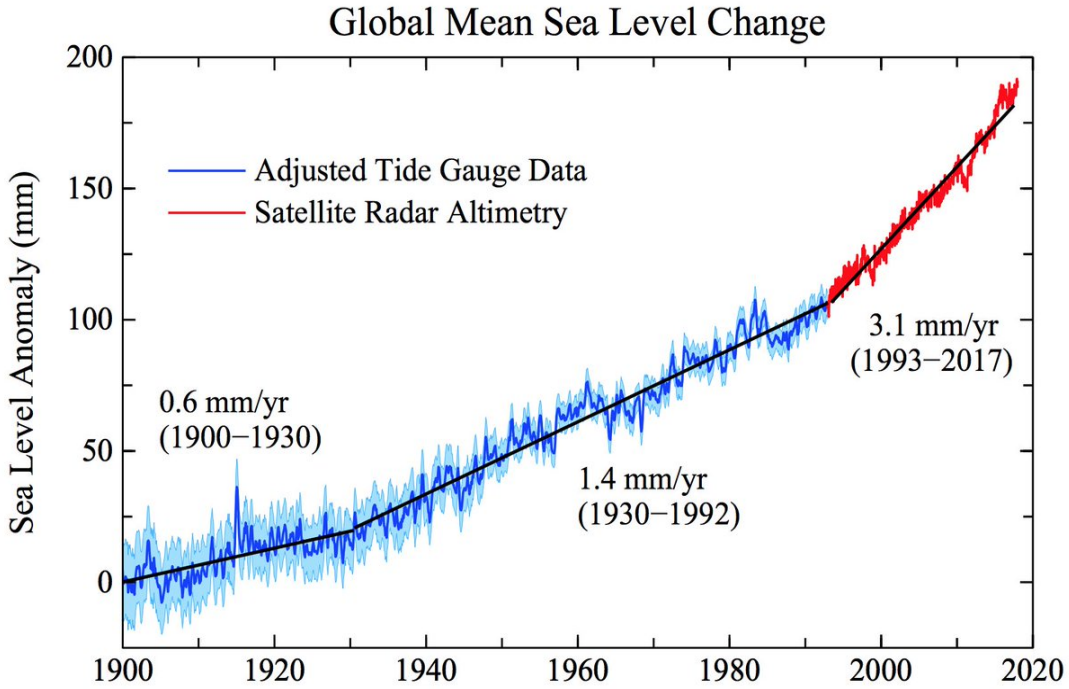

SLR tracking of radar altimetry satellites (Topex/Poseidon, Jason-1, and Jason-2) since 1992

70 mm rise in Mean Sea Level from 1992 to 2014 (22 years) yields rate of 3.17 ± 0.4 mm/yr

Contributors to Sea Level Change

- **variations in sea water temperature and salinity at all depths**
- **Tectonic changes to the water basin "shape"**
- **change of the ocean mass as a result of exchanges of water with the other surface reservoirs (atmosphere, continental waters, melting glaciers and ice sheets).**

Tide Gauge Drawbacks

- **Prior to the launch of the oceanographic satellites, tide gauges were used to estimate sea level rise**
- **Sparce geographical distribution provides very poor sampling of the ocean basins,**
- **They measure sea level relative to the land, hence recording vertical crustal motions that may be of the same order of magnitude as the sea level variation.**

Spatially Resolved Global Sea Level Rise

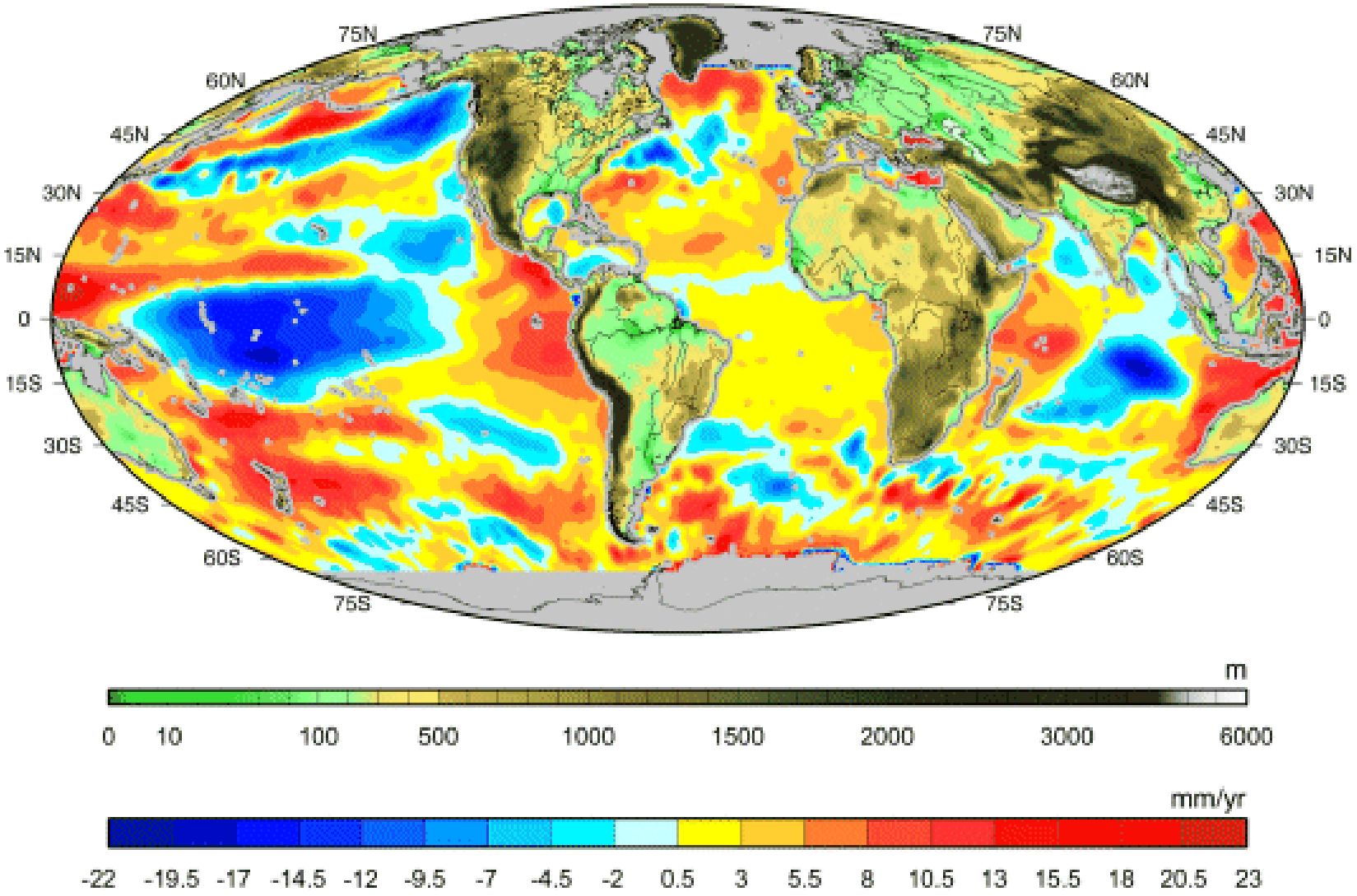

Sea Floor Topography from Sea Surface Altimetry

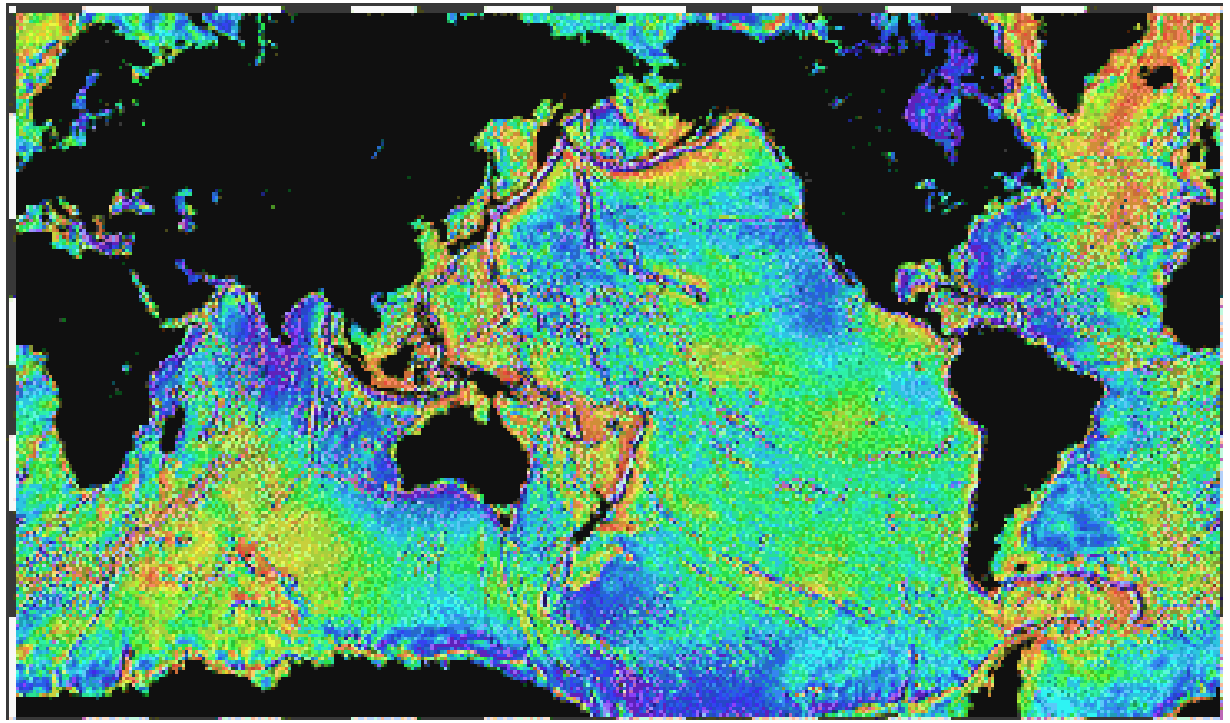

Ocean floor topography from Geosat and ERS-1 radar altimetry obtained with SLR tracking only
(David Sandwell and Walter Smith)

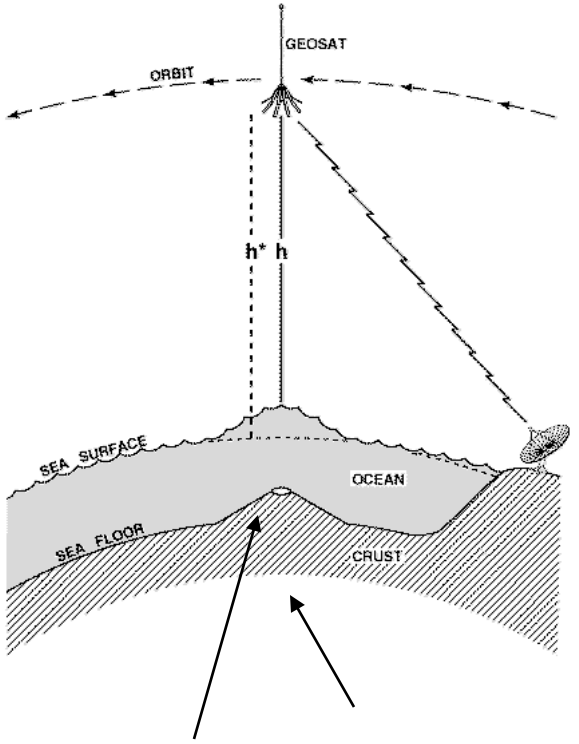

Approximately 1000:1 ratio in heights
(1 km sea mount creates ~1 m bump in sea level)

Spaceborne Laser Altimetry
(adapted from J. B. Abshire, GSFC)

Compared to microwave altimeters, lasers have much better spatial resolution and range precision. Until the launch of the SPL altimeter on ICESat-2 by NASA in September 2018 (60,000 surface measurements per sec or 6 beams at 10 kHz), all spaceborne laser altimeters utilized 2nd generation SLR technology (40 measurenents per sec for ICESat-1).

Apollo, - Moon
NASA (1971-1972)
Ruby laser,
5,000 shots

Clementine - Moon
LLNL/NRL (1994)
Nd:YAG laser,
~72,000 shots

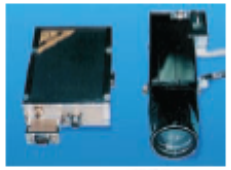

SELENE/LALT - Moon
Japan (2007-present)
Nd:YAG laser,

Chang'E - Moon
China (2007-present)
Nd:YAG laser

LRO/LOLA - Moon
NASA GSFC (2008-now)
Nd:YAG laser,
>1 Billion shots

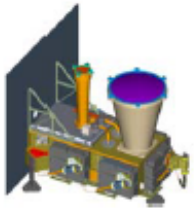

MGS/MOLA - Mars
NASA GSFC (1992, 1996 -2000)
Nd:YAG laser,
670 Million shots

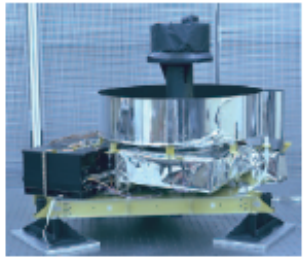

NEAR/NLR - Eros
JHU/APL (96-2001)
Nd:YAG laser,
11 Million shots

MESSENGER/MLA - Mercury
NASA GSFC (2004-2012)
Nd:YAG laser,
12M shots (planned)

Hayabusa -Itokawa
Japan (2003)

ICESat/GLAS - Earth
NASA GSFC (2003-2009)
3 Nd:YAG lasers
1.98 Billion shots

CALIPSO/CALIOP - Earth
NASA LaRC/ Ball Aerospace
(2006-present)
2 Nd:YAG lasers,
> 2B shots to date

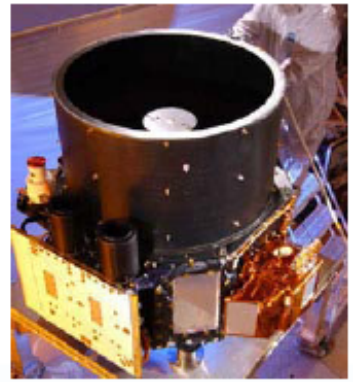

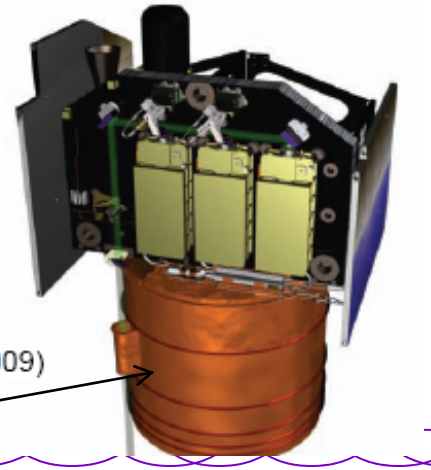

Lunar Orbiter Laser Altimeter (LOLA)

Color Code: red (highest EL), orange, yellow, green, blue (lowest EL)

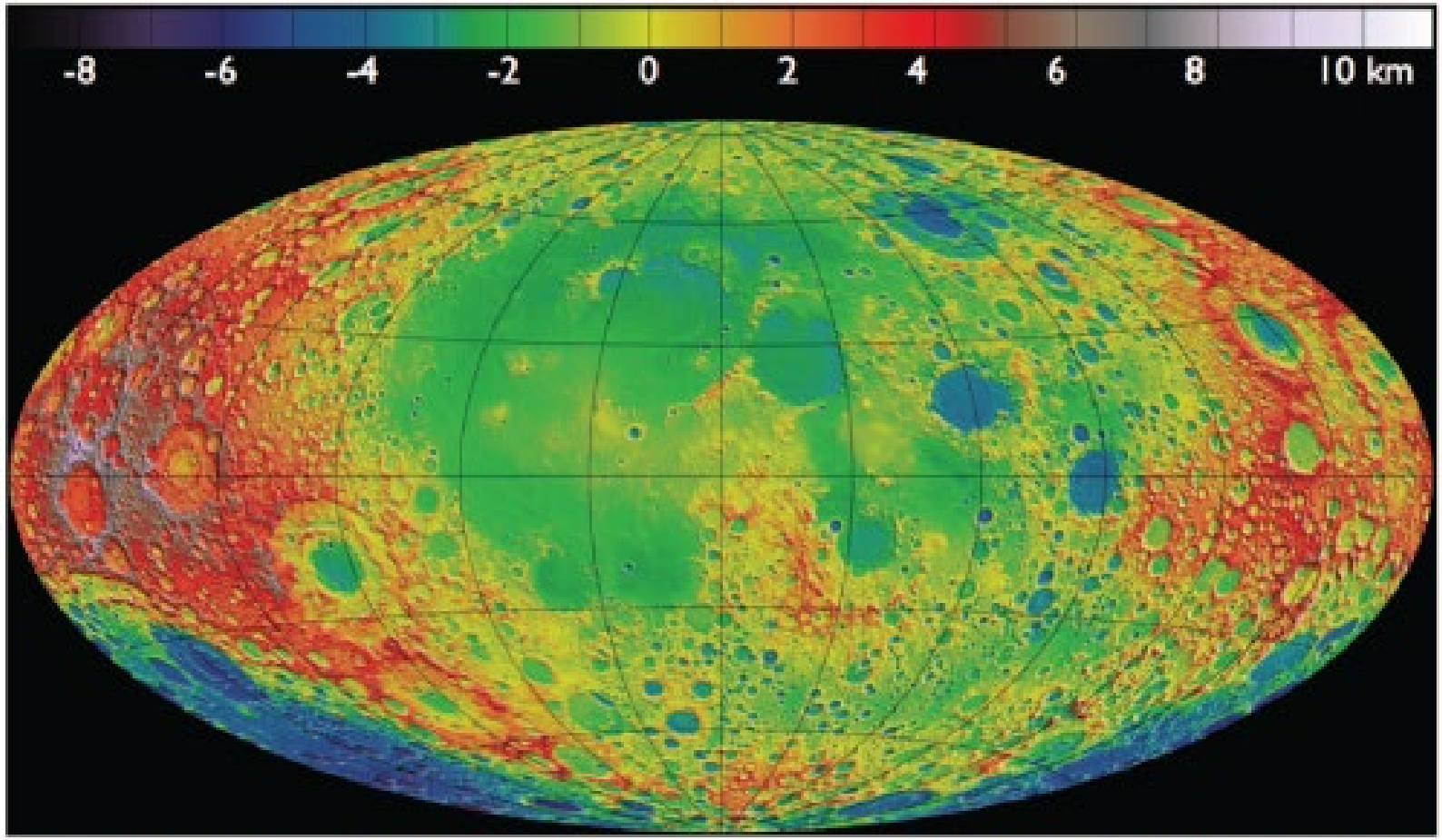

Equal-Area projection of lunar topography developed from1 billion LOLA measurements
Resolution: N/S ~20m; E/W ~0.1 deg (4.5km at equator, 200m at >85 Lat)

Mercury Topography from MLA

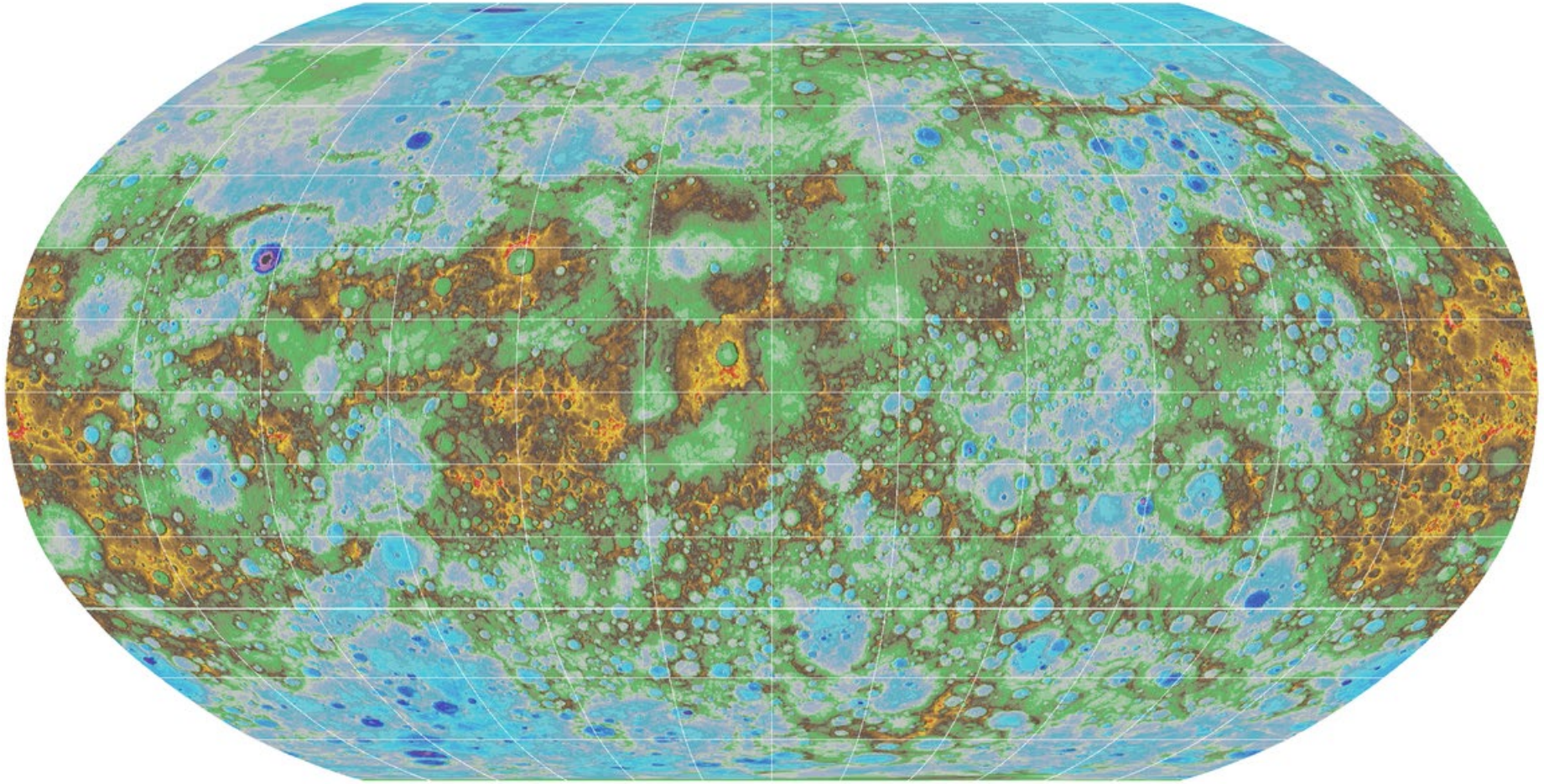

MLRO Map of Mars

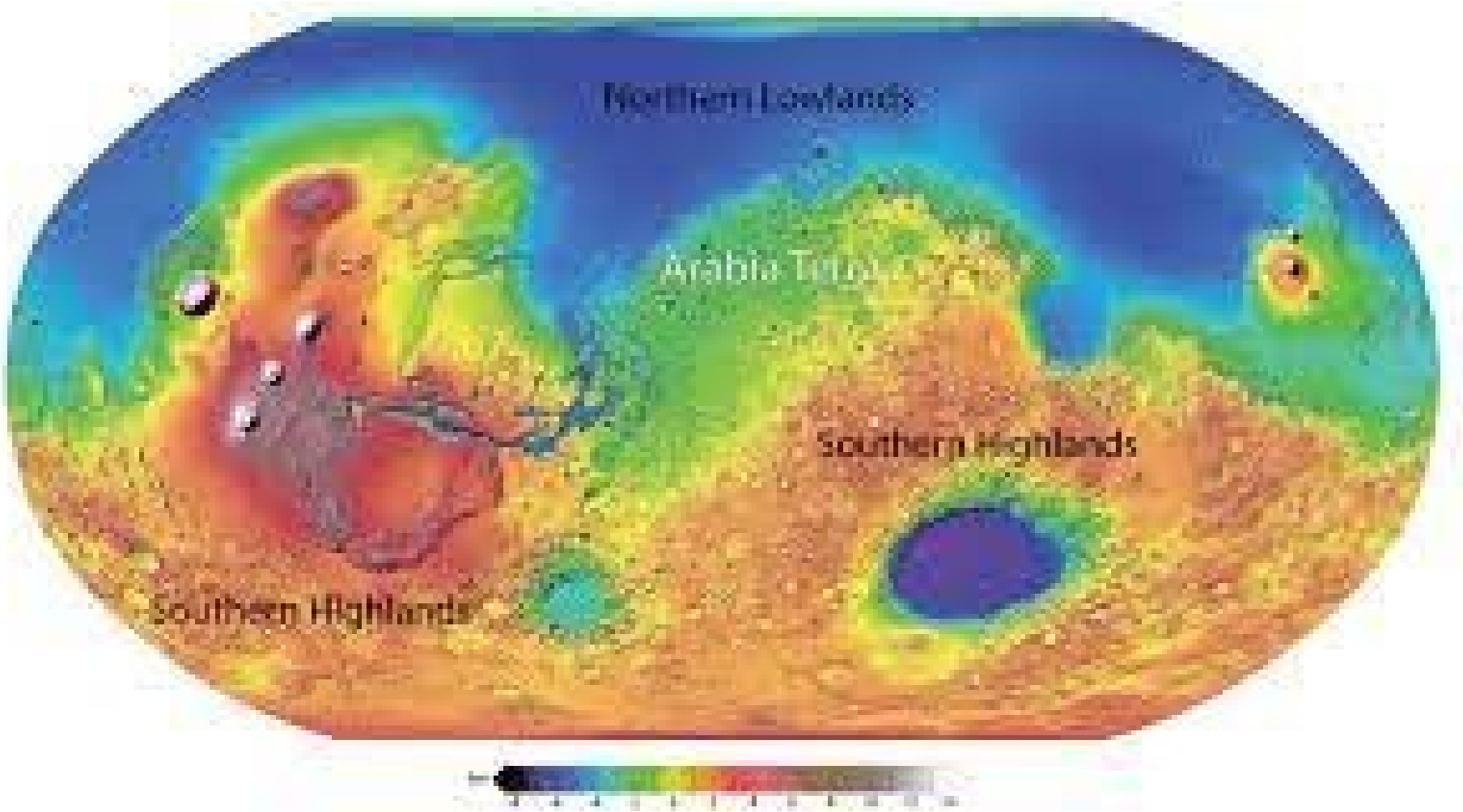

Single Photon Lidar (SPL)

J. Degnan, Remote Sensing, Sept. 2016.

- In 2001, my NASA SLR000 team successfully flew the "Microaltimeter", a terrain mapping lidar based on SPL ranging technology, i.e. low energy, ultrashort pulses operating at kHz rates whereas most existing laser altimeters had measurement rates of a few tens of Hz.
- In January 2003, I resigned my position at NASA/GSFC to serve as Chief Scientist at Sigma Space Corporation where, over the next decade, our team developed a commercial line of SPLs capable of making up to 6 million single photon range measurements per second (100 measurements per pulse at 60 kHz) from altitudes of 25,000 ft (7.5 km). In 2019, Sigma Space became a subsidiary of Hexagon Corp., based in Stockholm, Sweden.
- The 100 measurements per pulse were obtained by using a 10x10 array of single photon detectors which greatly improved the ground resolution of the lidar.
- A dual wedge scanner was developed to provide a contiguous map of the terrain while simultaneously overlapping the transmit and receive fields of view at any altitude by merely adjusting the scan speed.
- All of the spaceborne lidars on the previous chart were based on older multiphoton technology typically limited to tens of measurements per second. In 2006, I proposed an experimental 16 beam, 10 kHz SPL to fly on the ICESAT-2 Mission alongside a copy of the previously planned single beam 40 Hz ICESAT-1 lidar.
- In 2018, NASA launched the ICESAT-2 mission into a 500 km orbit with only the SPL lidar . The latter produces 6 beams (3 "strong" and 3 "weak") from a single laser operating at 10 kHz to produce 60,000 surface measurements per second. "Strong" beams contain 4 times the energy of the weak beam to provide better forest penetration.

SPL Map of Pacific Ocean Coastline at LaJolla CA

Sample:
Double Pass
AGL: 7500 ft
Velocity: 180 knots

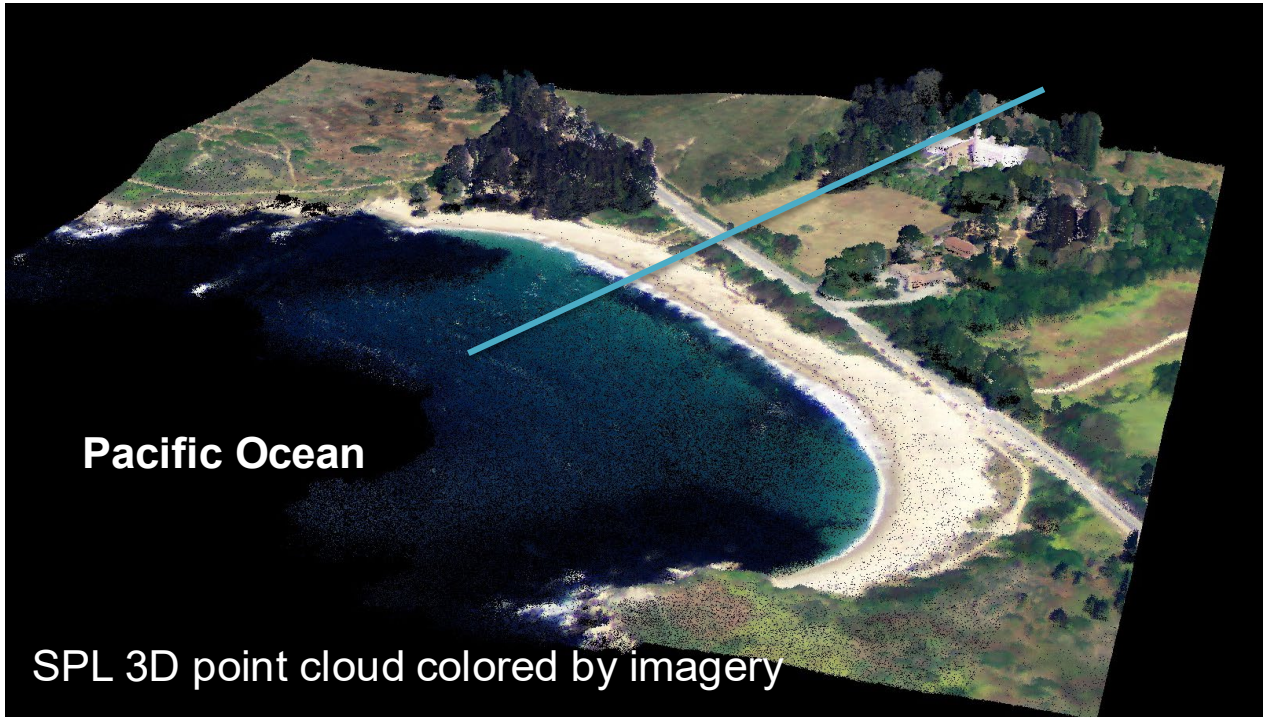

2D Profile

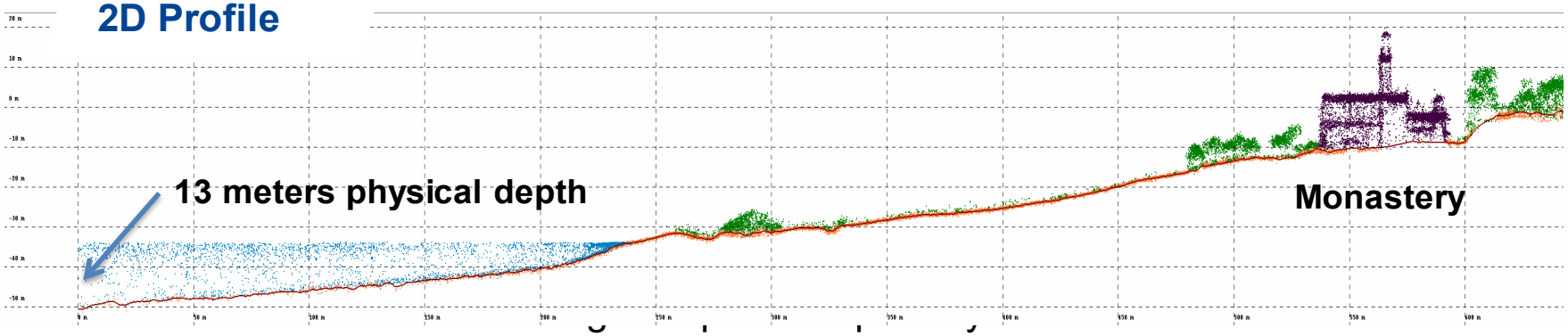

SPL Downtown Houston, Texas, USA

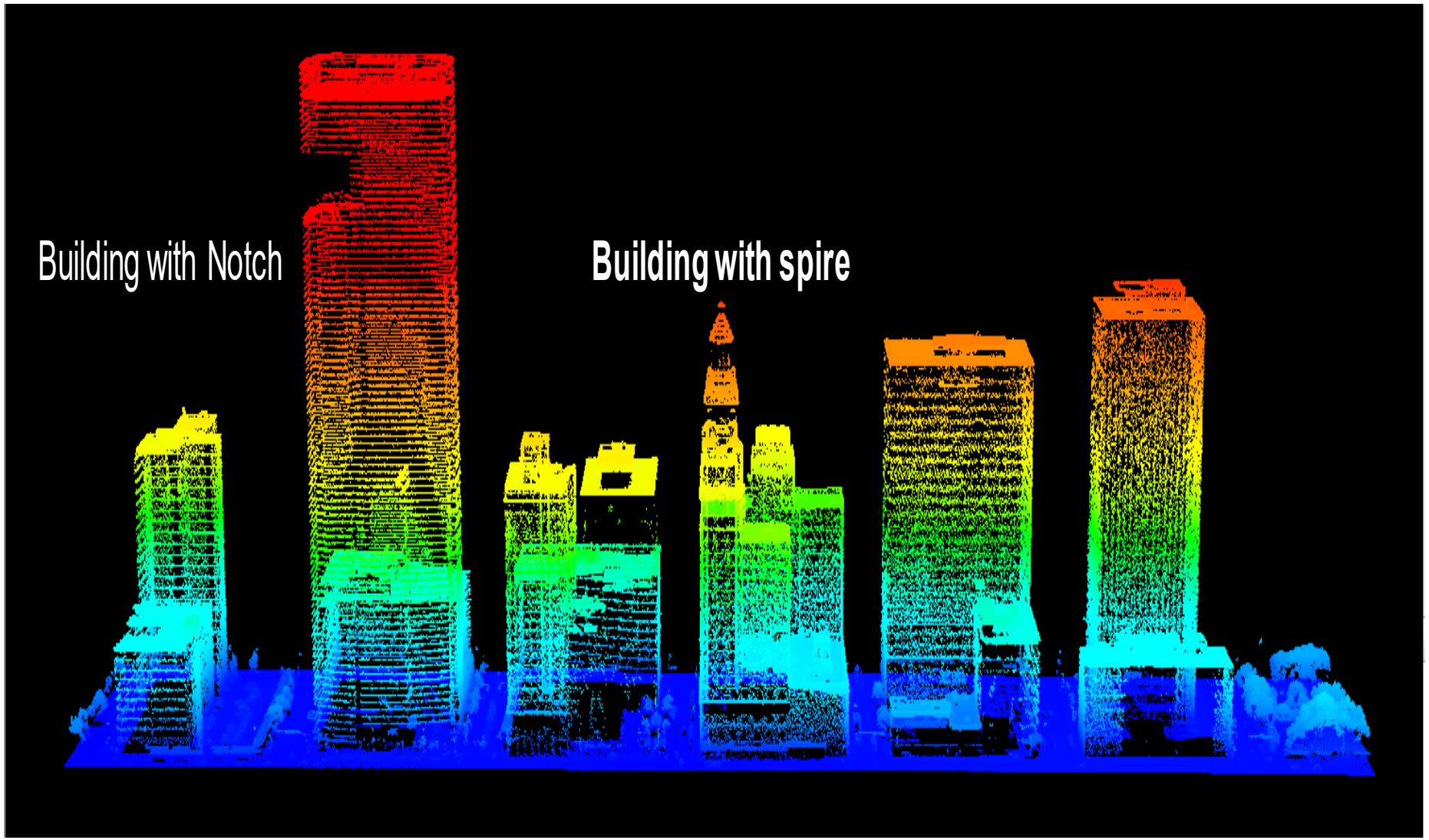

SPL Map of Manchester, England

SPL

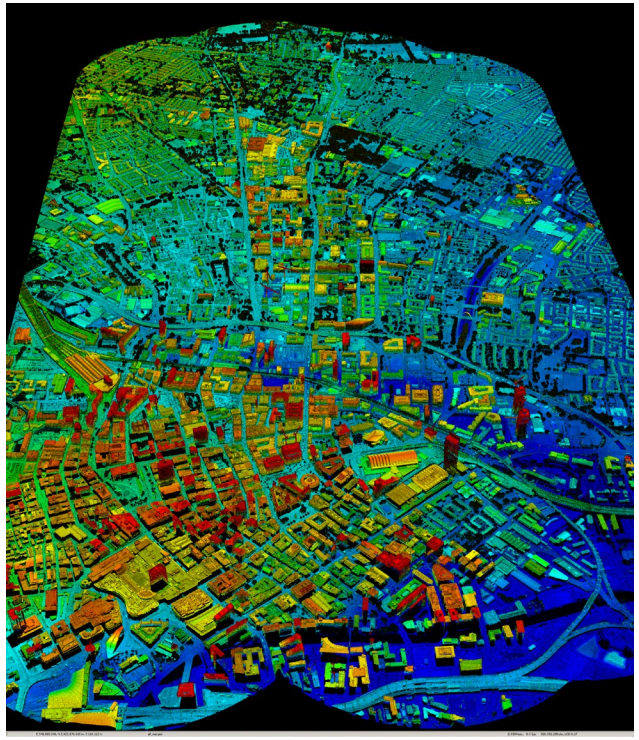

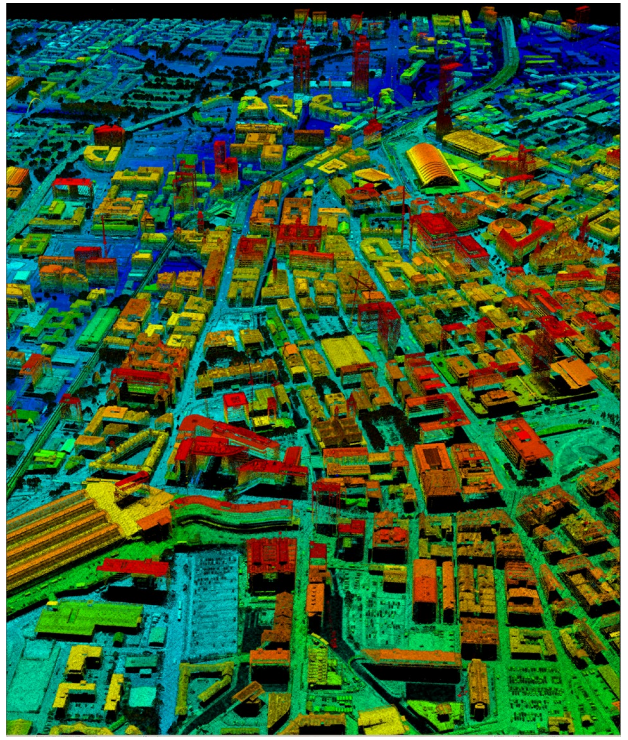

Lidar maps of Manchester, England . Four flight lines at 2.23 km altitude at 140 knots with 50% overlap resulted in a mean point density of 33 /m^2.

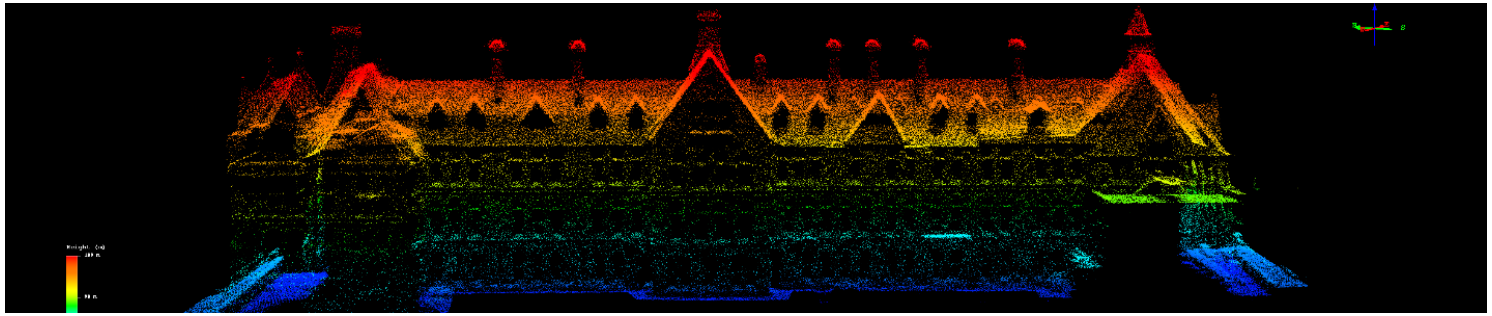

Closeup of a complex building.

Summary: Science Impact of SLR/LLR

- **Centimeter Accuracy Orbits**
  - Test/calibrate microwave navigation techniques (e.g., GPS, GLONASS, DORIS, PRARE)
  - Supports microwave and laser altimetry missions for global land topography, sea level, polar ice, and tree biomass measurements. (TOPEX/Poseidon, ERS 1&2, GFO, JASON, ICESats 1&2)
  - Support gravity missions (e.g. CHAMP, GRACE, Gravity Probe B)
- **Terrestrial Reference Frame**
  - Geocenter motion
  - Scale (GM)
  - 3-D station positions and velocities
- **Earth Gravity Field**
  - Static medium to long wavelength components
  - Time variation in long wavelength components due to mass redistributions within the solid Earth, oceans, cryosphere, and atmosphere
  - Free Air/Bougher gravity
  - Atmospheric Drag & Radiation Pressure Models
- **Geodynamics**
  - Tectonic plate motion
  - Regional crustal deformation at plate boundaries
- **Earth Orientation Parameters (EOP)**
  - Polar motion
  - Length of Day (LOD)
- **Global Time Transfer**
- **Laser Altimetry/3D Imaging Lidar**
- **Lunar Physics (LLR)**
  - Centimeter accuracy lunar ephemerides
  - Lunar librations (variations from uniform rotation)
  - Lunar tidal displacements
  - Lunar mass distribution
  - Secular deceleration due to tidal dissipation in Earth's oceans
  - Measurement of $G(M_E + M_M)$
- **General Relativity**
  - Test/evaluate competing theories
  - Support atomic clock experiments in aircraft and spacecraft
  - LLR validates Strong Equivalence Principle (SEP)
  - Constrain β parameter in the Robertson-Walker Metric
  - Constrains time rate of change in G (G-dot)
  - Measure Lense-Thirring Frame Dragging Effect (LAGEOS 1 and 2)
- **Solar System Reference Frame (LLR)**
  - Dynamic equinox
  - Obliquity of the Ecliptic
  - Precession constant
- **Interplanetary Ranging, Time Transfer and Communications**
  - Two-way interplanetary ranging and time transfer for improved navigation/control of spacecraft
  - Solar System Science and improved General Relativity Experiments
  - SLR stations and constellation can also support interplanetary laser communication development